What Drives Plate Motion?

Yongfeng Yang

Bureau of Water Resources of Shandong Province

Corresponding author: Yongfeng Yang (roufeng_yang@outlook.com)

Key Points:

- Plate driving force provides the first insights into the processes that yield plate tectonics
- We investigate to find that the two primary driving forces (ridge push and slab pull) cannot be accordance with observation
- An ocean-generating force driving mechanism is proposed to account for plate motion

Abstract

Plate motion is a remarkable Earth process and is widely ascribed to two primary driving forces: slab pull and ridge push. With the release of the first- and second-order stress fields since 1989, a few features of tectonic stresses provide strong constrain on these forces. The observed stresses are mainly distributed on the uppermost brittle part of the lithosphere. A modeling analysis, however, reveals that the stress produced by ridge push is dominantly distributed in the lower part of the lithosphere; Doglioni and Panza recently made an in-depth investigation on slab pull and found this force cannot be in accordance with observations. These findings of ridge push and slab pull suggest that there needs other force to be responsible for plate motion and tectonic stress. Here, we propose that the pressure of deep ocean water against the wall of continent yields enormous force (i.e., ocean-generated force) on the continent. The continent is fixed on the top of the lithosphere, this attachment allows ocean-generated force to be laterally transferred to the lithospheric plate. We show that this force may combine other forces to form force balances for the lithospheric plate, consequently, the African, Indian, South American, Australian, and Pacific plates obtain a movement of 4.52, 6.09, 2.11, 3.52, and 6.62 cm/yr, respectively. A torque balance modelling shows that the error between the movements calculated for 121 sample locations and the movements extracted from GSRM v.2.1 is less than 0.8 mm/yr in speed and 0.3^{o} in azimuth.

Plain Language Summary

Plate tectonics is one of the most significant paradigms in the 20^{th} century, it mainly describes the movements of a dozen different-sized plates over the Earth's surface. Exploring the plate driving forces is fundamental because it provides the first insights into the processes that yield plate tectonics. Slab pull and ridge push are presently thought to be the two primary driving forces. In this study, we model a vertical distribution of the stress caused by ridge push and recall the geometric, kinematic, and mechanical arguments of slab pull. These findings suggest these forces cannot be in accordance with observations and other force is needed. Approximately 71% of the Earth's surface is covered with ocean water. Ocean water exerts pressure everywhere, this pressure against the walls of continents creates enormous force on continents. In this study, we investigate the geometry of this force and its distribution around the

lithospheric plates. By a semianalytical model, we find this force may combine collisional, shear, and basal friction forces to form force balances for plate, consequently, plate motion can be realized. This newly proposed force expands our understanding of the dynamic interaction between the lithosphere and ocean.

1 Introduction

One of the most significantly achievements in the 20th century was the establishment of the plate tectonics , which developed from the previous concept of continental drift (Wegener, 1915 and 1924). Plate tectonics mainly describes the motion of a dozen different-sized plates that connect with each other to form a giant "jigsaw puzzle" over the Earth's surface. The evidence supporting this motion includes shape fitting of the African and American continents, a coal belt crossing from North America to Eurasia, identical directions of ice sheet movement in southern Africa and India, and speed measurements made by the Global Positioning System (GPS). In addition, paleomagnetic reversals in oceans (Hess, 1962; Vine and Matthews, 1963) reflect sea-floor spreading, and studies of the Hawaii-Emperor seamount chain have shown that the chain is actually a trace of the lithosphere rapidly moving over relatively motionless hotspots (Wilson, 1963; Raymond et al., 2000), which further confirms the Earth's surface motion. During the past 50 years, the understanding of plate motion has expanded greatly. Plates were found to have been periodically dispersed and aggregated in the Mesozoic period, accompanied by 5-6 significant astronomical events (Cande and Kent, 1992; Cande et al., 1989; Ma et al., 1996; Wan, 1993; Hibsch et al., 1995). The speed and direction of plate motion supported by paleomagnetism and deformation in the intraplate regions exhibited various styles over geological time (Wan, 2018). Global measurements of tectonic stresses revealed a strong correlation with plate motion, and the observed stresses may be used to constrain the forces that act on the plates (Zoback et al., 1989; Zoback, 1992; Bott and Kusznir, 1984; Zoback & Magee, 1991; Richards, 1992; Sperner et al., 2003; Heidbach et al., 2016; Heidbach et al., 2007; Heidbach et al., 2010; Heidbach et al., 2018).

Exploring the plate driving forces is important because it provides the first insights into the processes that yield plate tectonics. Throughout the history of plate tectonics, a large number of forces have been postulated to explain plate motion. Forces include centrifugal and tidal forces, ridge push, slab pull, basal drag, slab suction, mantle

plume, geoid deformation, and the Coriolis force (Wegener, 1915; Hales, 1936; Holmes, 1931; Pekeris, 1935; Runcorn, 1962a,b; Wilson, 1963; McKenzie, 1968; McKenzie, 1969; Morgan, 1971; Morgan, 1972; Turcotte and Oxburgh, 1972; Forsyth & Uyeda, 1975; Oxburgh and Turcotte, 1978; Spence, 1987; White & McKenzie, 1989; Richards, 1992; Vigny et al., 1992; Bott, 1993; Tanimoto & Lay, 2000; Conrad & Lithgow-Bertelloni, 2002; Turcotte and Schubert, 2014). Slab pull is derived from a cold and dense sinking plate that uses its weight to pull the remaining plate to which it is attached. Ridge push is usually treated either as a boundary force or a body force . As a boundary force, ridge push is derived from a "gravity wedging" effect of warm, buoyant mantle upwelling beneath the ridge crest and acts at the edge of the lithospheric plate. In contrast, as a body force, ridge push is derived from the horizontal pressure gradient of the cooling and thickening of the oceanic lithosphere and acts over the area of the oceanic portion of a given plate. As these two forces act on the edges of plates, they are often termed boundary forces. Basal drag (i.e., basal shear traction) is thought to be caused by the viscous moving asthenosphere along the bottom of the lithosphere. Mantle plume represents the rising hot mantle flow that originated from the core-mantle boundary (Morgan, 1971; Morgan, 1972; Wilson, 1963).

Early studies of deformation modeling and torque balance analysis tended to agree that ridge push and slab pull are important for plate motion, whereas basal drag provides resistance instead of driving force (Forsyth & Uyeda, 1975; Solomon et al., 1975; Chapple and Tullis, 1977; Richardson et al., 1979; Wortel and Cloetingh, 1981; Cloetingh and Wortel, 1986; Richardson and Cox, 1984; Richardson and Reding, 1991; Stefanick and Jurdy, 1992). Subsequent researches with complicated physical models yielded an improved understanding: buoyancy anomalies within the lithosphere, crust, , and mantle act as the principal drivers, whereas viscous dissipation within the lithosphere and at its base and shear along thrust faults at collision zones resist plate motion (Conrad and Hager, 1999; Conrad and Lithgow-Bertelloni, 2002; Stadler et al., 2010; Lithgow-Bertelloni and Richards, 1995; Becker and O'Connell, 2001; Zhong, 2001; Bird et al., 2008; Becker and Faccenna, 2011; Ghosh et al., 2013; Coltice et al., 2017). That is, besides slab pull and ridge push, the lithosphere and mantle feed plate motion in some way. For example, the lithosphere’s density variation forms a lateral pressure gradient by which plate motion is driven. The sinking slab inserts into the deeper mantle while the hot mantle flows (i.e.,

plumes) originated from the core-mantle boundary rise up to the top of the asthenosphere; this process of upwelling and downwelling causes the large-scale circulation of plate and mantle (i.e., whole mantle convection). A more detailed description of whole mantle convection is discussed in these works (Coltice et al., 2017; Bercovici et al., 2015). On the whole, the efforts made in the past 40 years tend to agree that ridge push and slab pull are the primary plate driving forces, whereas mantle plumes that act as a driving force still remains controversial.

2 What's the problem of the primary driving forces

2.1 Ridge push

Tectonic stresses are caused by the forces that act on the plates (Middleton and Wilcock, 1996), and they in turn provide constrain on the plate driving forces. With the first release of the first- and second-order stress fields (Zoback et al., 1989; Zoback, 1992; Zoback & Magee, 1991), it becomes evident in the World Stress Map (WSM) that the maximum horizontal compressional stress S_H in North America, South America and Europe has the orientation that is predominately subparallel to either the relative or absolute plate motions (Richardson, 1992; Müller et al., 1992; Zoback, 1992). Due to this coupling of stress orientations and plate motions, the first-order intraplate stress patterns are concluded, mainly by means of torque analysis, to be caused by the same forces that drive plate motion, especially slab pull, ridge push, collisional forces, trench suction, and traction at the base of the lithosphere (Richardson, 1992; Zoback, 1992; Grünthal and Stromeyer, 1992; Gölke and Coblentz, 1996;Zoback and Zoback, 1991; Zoback and Burke, 1993; Zoback et al., 1989). Subsequent releases of the stress field (Heidbach et al., 2016; Sperner et al., 2003; Heidbach et al., 2010; Heidbach et al., 2007; Heidbach et al., 2018) and modeling studies that reproduce plate tectonics (Ghosh et al., 2013; Richards, 1992; Stadler et al., 2010; Becker and O'Connell, 2001; Bird et al., 2008; Ghosh and Holt, 2012; Lithgow-Bertelloni and Guynn, 2004; Alisic et al., 2012;) agree with this conclusion. Yet, this match in orientation and style (i.e., compressional or extensional) between the stresses produced by these forces and the observed stresses is limited to the lithosphere's surface, i.e., the lithosphere is treated as a thin "shell" that is similar to membrane, the related forces are acted at the edges of the lithospheric plates and their base to produce the stresses, the resultant stresses are projected on the surface of the

plate, and then, these stresses are compared with the observed stresses in the WSM. Consequently, an examination of the consistency between the produced stresses and the observed stresses across the entire thickness of the lithosphere is commonly absent. In fact, the first release of the first- and second-order stress fields (Zoback et al., 1989; Zoback, 1992; Zoback & Magee, 1991) revealed another important feature of the tectonic stresses: the observed stresses are mainly concentrated on the uppermost brittle part of the lithosphere (which is ~ 40 km depth), except for some portions of the continent dominated by high topography. This vertical distribution feature of tectonic stresses is often not included by these modeling studies (i.e., Ghosh and Holt, 2012; Lithgow-Bertelloni and Guynn, 2004). As mentioned above, ridge push is treated either as a boundary force or a body force. As a boundary force, it is derived from a "gravity wedging" effect of warm, buoyant mantle upwelling and acts at the edge of the lithospheric plate. Relying on a model that is similar to Figure 1 (top), Turcotte and Schubert (2002) expressed ridge push force as $F_{RP}=g\rho_m\alpha_v(T_1-T_0)[1+2\rho_m\alpha_v(T_1-T_0)/\pi(\rho_m-\rho_w)]\kappa t$, where g, ρ_m, ρ_w, T_1, T_0, α_v, κ, and t are respectively gravitational acceleration, mantle density, water density, mantle temperature, temperature at plate surface, thermal expansivity, diffusivity, and age of seafloor. Since this expression was made through some mathematic substitution and integrations, and both mantle density and mantle temperature linearly increase with depth, these aspects determine that ridge push force would increase with depth. In other words, the minimum ridge push force, which is zero due to $T_1= T_0$, would appear at the top of the oceanic ridge, whereas the maximum ridge push force would appear at the bottom of the oceanic ridge.

We here employ a simple model (Figure 1 (bottom)) to examine the vertical distribution of the stresses produced by ridge push force. The model consists of continental Plate A and oceanic Plate B. The plates are straight meaning the Earth's curvature is not considered. Plate A is assumed to be homogeneous and isotropic, and its thickness is given as 100 km. Along the horizontal direction, Plate B exerts a collisional force F_c on Plate A, this force is resistive and uniformly exerted on the section *GH* of 90 km length; the oceanic ridge exerts a push force F_{RP} on the section *JI* of 85 km length, this force is driving and increases with depth; the mantle exerts a friction force F_b on the base of Plate A, this force is resistive and shears the section *HI* of 5, 000 km length. These forces realize a horizontal force balance for the section

GHIJ. Along the vertical direction, Plate A is supported by the mantle, its gravity is balanced out by the supporting force from the mantle. Finite element analysis software (i.e., Abaqus) is used to resolve the resultant stress across the section *GHIJ*. The bottom of the section *GHIJ* is given a remote boundary condition. As the upper part of the lithospheric plate is elastic and brittle whereas the lower part is plastic and ductile, this reality allows us to assume that the physical property of section *GHIJ* is vertically transited from elasticity to plasticity. The inputs include the vertical pressure caused by the section *GHIJ*'s weight and the lateral pressures caused these forces F_{RP}, F_{b}, and F_{c}. The outputs include two sets of data: one is the stress produced by the vertical pressure alone, and the other is the stress produced by a combination of the vertical pressure and lateral pressures. The two-dimensional frame allows us to obtain a horizontal stress S11 and a vertical stress S22. Elastic modulus, Poisson ratio, and the rock's density of the section *GHIJ* are given as 100,000 Mpa, 0.3, and 2,690 kg/m^3, respectively. F_{RP} is given as 4.0×10^{12} N m^{-1}, this amplitude is generally accepted (Turcotte and Schubert, 2004). F_b and F_c are assumed to be 80% and 20% of the F_{RP}, which are 3.2×10^{12} N m^{-1} and 0.8×10^{12} N m^{-1}. To test a variation of the resultant stresses when the resistive forces are adjusted, F_b and F_c are again assumed to be 50% and 50% of the F_{RP}, which are 2.0×10^{12} N m^{-1} and 2.0×10^{12} N m^{-1}. And then, these forces are applied to the related sections, resulting in pressures.

The produced stresses are exhibited in Figure 2. We find that the maximum horizontal stress S11 is compressional and mostly concentrated on the lower part of the section *GHIJ*. This style is dominant even if the magnitude of both F_b and F_c is adjusted. Kusznir and Bott (1977) argued that, because of the ductile nature of the lower part of the lithosphere, there would be a redistribution of any stress applied to the whole lithosphere and result in a stress amplification in the upper brittle part of the lithosphere. This view is based on an assumption that force is uniformly exerted on the side of the lithospheric plate, but the reality is ridge push force would increase with depth, consequently, the redistribution of the stress and its amplification are not applicable to ridge push force. Instead, we have considered the ductile nature in the modeling, but no evidence is found to show a stress amplification in the upper brittle part of the section *GHIJ*. This analysis of the vertical distribution of horizontal stress indicates that the stress caused by slab pull cannot be in accordance with the observed stress.

Look over the plate's shape around the globe, it is evident that the eastern coastline of the American continent is approximately subparallel to the Atlantic ridge where it is the plate's boundary, and the coastline of the Australia's continent is subparallel to the boundary of the Australian plate. However, the length of the coastline of the American continent is greater than that of the Atlantic ridge, whereas the length of the coastline of the Australian continent is far less than that of the boundary. This pattern is also clear for the Indian plate. This discrepancy suggests that the plate driving force is likely to be a force arising from the coastline that pulls the continental plate rather than a force arising from the boundary (ridge) that pushes the continental plate.

All plates are steadily moving over the Earth's surface, this reality indicates that there are the separation and approach between plates. The separation would result in a gap between two plates. If the gap were deep enough, it would allow magma to erupt and form a mid-ocean ridge (MOR). In this respect, the MOR may be the result of plate motion. Nowadays, the MOR is treated as the cause of the plate driving force. This treatment leads to the chicken-or-egg question: which came first? In physics, the object that exerts force must clearly differentiate from the object that accepts this force. Some people argue that once subduction and spreading are initiated, plates may drive themselves as part of large circulation of the mantle and lithosphere, by which the chicken-or-egg question is resolved. This argument cannot be convincing. Ridge push contributes to not only oceanic plates but also continental plates, but continental plates are not sinking, they cannot take part in the large circulation, consequently, the

chicken-or-egg question remains for the ridge push of continental plates.

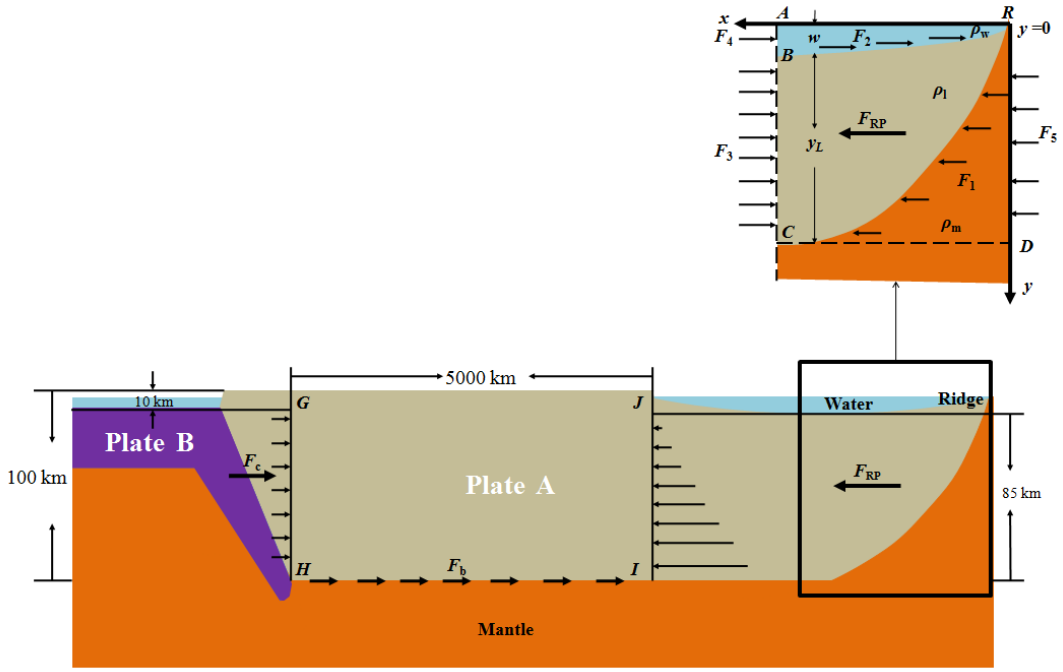

Figure 1. Modeling the distribution of ridge push, basal friction, and collsional force around a continental plate.

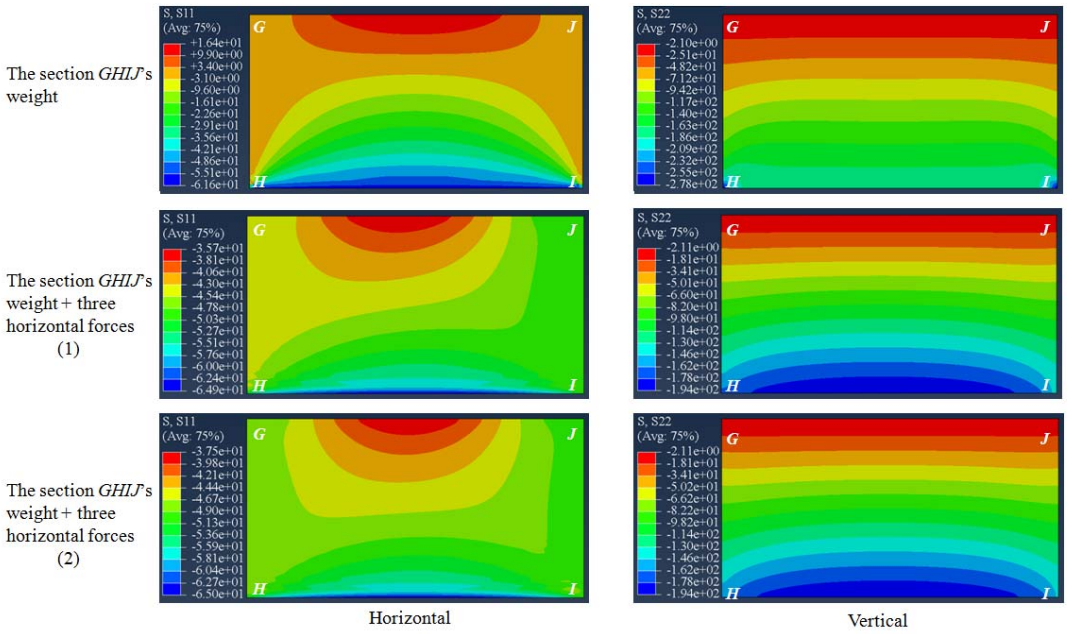

Figure 2. Stresses caused by a combination of ridge push, basal friction, and collisional force within a modelled section of continental plate. In the model of the section *GHIJ*'s weight + three horizontal forces (1), F_b and F_c are 80% and 20% of the

F_{RP}, respectively; whereas in the model of the section *GHIJ*'s weight + three horizontal forces (2), F_b and F_c are 50% and 50% of the F_{RP}, respectively.

2.2 Slab pull

Slab pull is conceived as a "negative" buoyancy of sinking slab to drive the motion of the oceanic plate (e.g., Conrad & Lithgow-Bertelloni, 2003). However, since this force was proposed, its validity remains debated. Doglioni and Panza (2015) recently carried an in-depth investigation on slab pull, some of their findings include:

1) As demonstrated by Cruciani et al. (2005) that the slab's dip is unrelated to the age of the oceanic lithosphere, consequently, the negative buoyancy that increases with age and is determined by the cooling oceanic lithosphere cannot control the slab's dip;

2) It is assumed that the eclogitization within a slab would increase the lithosphere's density. Nevertheless, eclogitization is mostly distributed in the oceanic crust of 6~8 km depth, this transformation does not occur in the remaining lithospheric mantle of 60~80 km depth. It is possible that a little part of the slab's density can increase, but the majority of the slab's density does not change;

3) It is often asked why the lithosphere would subduct. This issue arises when an oceanic hydrated and serpentinized lithosphere is involved (Ulmer & Trommsdorff, 1995). Without being metamorphosed by the subduction process, the oceanic lithosphere would not denser than the surrounding rocks. As pointed out by Panza et al.(2007), the serpentinized LID often occurs along transform faults and ridges, therefore, it is lighter than the asthenospheric mantle, a question is then how plates can be pulled?

4) Most of the slabs is affected by down-dip compression, this influence is limited to a depth of below 300 km (Isacks & Molnar, 1971). Frepoli et al. (1996) showed that most of slabs may appear at shallower depth, this situation requires a slab to be forced to sink rather than positively to sink;

5) Although there is no slab for continental plates, these plates still move, the movements of North America, South America, and Africa are the examples (Gripp & Gordon, 2002). Trench suction is widely used to account for these movements, but the mantle that is beneath both South and North America is moving eastward (Russo & Silver, 1994; Bokelmann, 2002), this trend is object to the kinematics required by the trench suction model;

6) In the hot spot reference frame it seem like that plate velocities are inversely proportional to the low velocity zone's viscosity and not related to both the age of the downgoing lithosphere and the length of the subduction zones. For example, the Pacific plate is the fastest moving plate, but the viscosity of the asthenosphere beneath this plate is rather low (Pollitz et al., 1998; Gripp & Gordon, 2002);
7) The vertical velocity of plates (subduction-related uplift or subsidence along plate boundaries) is far slower than the horizontal one (Kreemer et al., 2002), this situation implies that the vertical motions of plates are rather passive. Also, an analysis of kinematics reveals that subduction rate appears to be controlled by horizontal plate motion; For instance, along E- (or NE-) directed slabs, the convergence rate is faster than the subductionand, therefore the subduction cannot be the energetic source of plate motion;
8) When one addresses the plate motion relative to the underlying mantle, the slab might move out of the mantle, the slab is sinking just because there is faster upper plate which overrides it (El Gabryet al., 2013);
9) The strength of the oceanic lithosphere is low (e.g., about 8×10^{12} N m^{-1})(Liu et al., 2004), this reality means that the oceanic lithosphere is able to resist a force that is smaller than slab pull (about 3.3×10^{13} N m^{-1})(Turcotte & Schubert, 2002). If slab pull is the primary driving force for the Pacific plate, the argument of strength above would require a stretching for the Pacific plate before slab pull drives this plate to move;
10) Brandmayr et al. (2011) and El Gabry et al. (2013) recently investigated the geodynamis in the Mediterranean region. Their findings of Vs and ρ distribution with depth suggest that slabs are less dense than the surrounding mantle and no evidence is found to support slab pull.
These arguments on slab pull leads to a conclusion that slab pull cannot drive the oceanic plate to move (Doglioni and Panza, 2015). This conclusion is further strengthened by Faccincani et al. (2021). These authors revealed the lithospheric mantle's density structure can be affected by the variations in thermal regimes and bulk composition, their results suggest that the lithospheric mantle is not denser than the underlying asthenospheric mantle. A difference of density between the lithospheric mantle and underlying asthenospheric mantle means that the oceanic plate, which mostly consists of the lithospheric mantle, is unlikely to sink forming a "negative" buoyancy to drive plate motion.

As mentioned earlier in the section 1, the latest understanding of plate dynamics is the buoyancy anomalies within the lithosphere, crust, and mantle act as the principal drivers of plate motion. In short, the dynamic source of plate motion is ascribed to the crust, lithosphere, and mantle. The terrestrial planets (Venus, Mercury, and Mars) share similar formation procession and interior structure (i.e., crust, mantle, and core) with the Earth, and also undergo same spatial surrounding (i.e., asteroid impact) as the Earth does. Therefore a question is why there is plate motion on the Earth, except for these terrestrial planets? This discrepancy of plate motion distribution, together with these issues of ridge push and slab pull that we demonstrate above, implies that some key factor of the Earth, which is still unrecognized to us today, determines plate motion.

3 An ocean-generating force driving mechanism for plate motion

Ocean water covers approximately 71% of the Earth's surface, and its total volume is almost 1.35 billion km^3, with an average depth of nearly 3,700 meters. Geochemical study of zircons suggests liquid water has existed for more than 4 Gy ago (Mojzsis et al., 2001; Bercovici et al., 2015; Valley et al., 2002). Ocean water is supported by the upper part of the lithosphere, this loading allows ocean water's weight to be vertically transferred to the lithosphere. The impact of ocean water on the isostatic balance and heat process of the lithosphere has been widely discussed (Bercovici et al., 2015; Fleitout and Froidevaux, 1983; Osei Tutu et al., 2018; Ricard et al., 1984; Steinberger et al., 2001; Lithgow-Bertelloni, 2014; Ghosh and Holt, 2012; Naliboff et al., 2012). It is already recognized that there is no plate tectonics on the other terrestrial planets (e.g., Mars and Venus), this absence is typically ascribed to the lack of liquid water, because Mars' water possibly appeared in liquid form in its early history and Venus's water has disappeared through a runaway greenhouse (Squyres et al., 2004). Nevertheless, the mechanism by which liquid water contributes to plate tectonics remains enigmatic (Bercovici et al., 2015). A view is the Earth's surface is cooled by liquid water, since the Earth's temperate in the formation of plate tectonics needs to be stabilized by a negative feedback (Bercovici et al., 2015; Walker et al., 1981; Berner, 2004). Nevertheless, from a view of fluid mechanics, ocean water (as liquid) can exert pressure everywhere, this pressure against the wall of the continent creates enormous force on the continent. As the continents are fixed on the top of the

lithosphere, and the lithospheric plates connect to each other, this attachment of the continents to the top of the lithosphere allows this force to be laterally transferred to the lithospheric plates.

3.1 A force balance solution for plate motion

3.1.1 Forces acting on the continental plate

A liquid can exert pressure on the wall of a container that holds it. According to Figure 3(top), the pressure generated on the wall of a cubic container may be written as $P=\rho g y/2$, and the application of this pressure across the wall yields a force. This force may be expressed as $F=PS=\rho g y^2 x/2$, where S is the wall's area, g and ρ are the gravitational acceleration and liquid's density , respectively, and x and y are the liquid's width and depth, respectively, in the container. Referring to the real world, ocean basins are naturally gigantic containers, and their depths are often more than a few kilometers and vary from one place to another. All of these factors imply that oceans can generate enormous pressure everywhere and that this pressure is unequal among oceans. Furthermore, the application of pressure against the ocean basin's walls, which consist of the continents, can yield enormous unequal forces on the continents. Geometrically, ocean pressure is always exerted vertical to the continental slope, by which a normal force is formed. This normal force is called ocean-generated force, which may be further decomposed into horizontal force and vertical force. As the continent attaches to the upper part of a continental plate, ocean-generated force can be laterally transferred to the continental plate. Subsequently, we list the plausible forces that act on a sample continental plate (Figure 3(bottom)), and discuss the physical nature of these forces.

These forces can be classified into two categories: the forces acting on the parts of the continent that connect to oceans and those acting at both the bottom surface of the continental plate and the parts of the continental plate that connect to adjacent plates. The forces acting on the parts of the continent that connect to the ocean derive from ocean pressure and are treated as ocean-generated forces, denoted F_R on the right and F_L on the left. The horizontal forces decomposed from these forces are denoted F_R' on the right and F_L' on the left. The force acting on the continental plate's bottom surface arises from a coupling between the plate and underlying viscous asthenosphere. It is called the basal friction force and denoted as f_{base}. As addressed by Forsyth & Uyeda

(1975), if there is thermal convection in the asthenosphere, f_{base} would be a driving force (Runcorn, 1962a, b; Turcotte & Oxburgh, 1972; Morgan, 1972). If, instead, the asthenosphere is passive relative to plate motion, f_{base} would be a resistive force. Here, we assume f_{base} is a resistive force. The forces acting on the parts of the continental plate that connect to adjacent plates arise from a physical connection of the continental plate and adjacent plates. Given that the continental plate moves towards the right, they are called the collisional force from the plate on the right side, the shearing force from the plate on the far side, the shearing force from the plate on the near side, and they are denoted f_{right}, f_{far}, and f_{near}, respectively. Oceanic ridge represents a boundary of two separating plates, we assume there is no pull force from the plate on the left side. Then, a combination of all of these forces for the continental plate in the horizontal direction may be written as

$$F = (F_L' - F_R') - (f_{base} + f_{right} + f_{far} + f_{near}) \qquad (1)$$

where the first term ($F_L' - F_R'$) denotes the final horizontal force, which provides a dynamic source for the continental plate, the second term ($f_{base} + f_{right} + f_{far} + f_{near}$) denotes the total resistive force, which hinders the continental plate's movement. Here, we indicate ($F_L' - F_R'$) as F_{final} and ($f_{base} + f_{right} + f_{far} + f_{near}$) as $F_{resistive}$. F_L' and F_R' may be further written as $F_L' = 0.5\rho g L h_L^2$ and $F_R' = 0.5\rho g L h_R^2$, where ρ, g, L, h_L, and h_R are the density of water, gravitational acceleration, ocean width that fits the continent's width, ocean depth at the left, and ocean depth at the right, respectively.

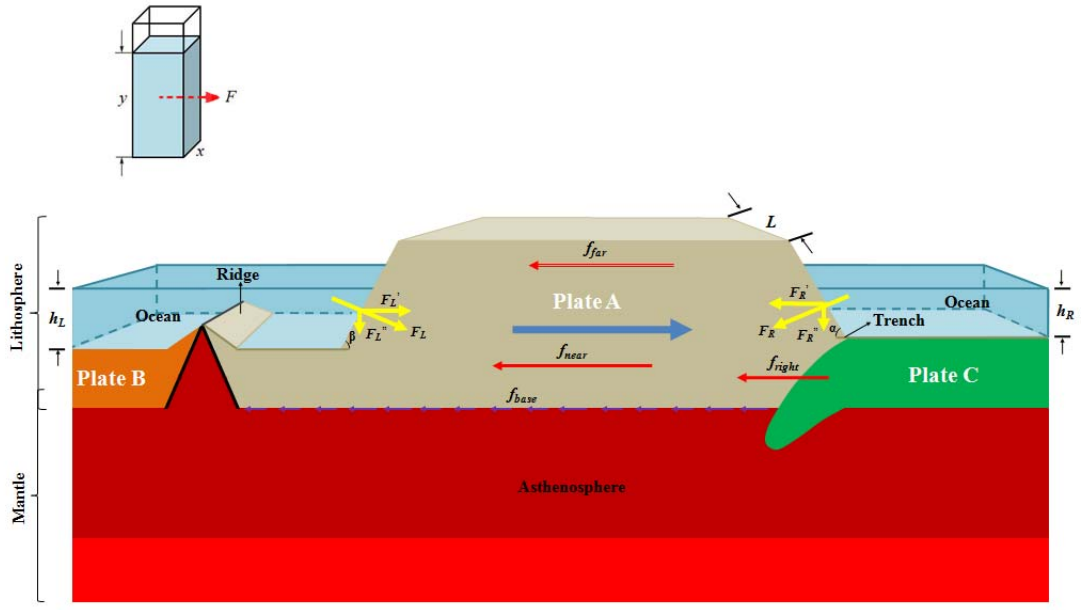

Figure 3. Modeling the dynamics of a continental plate. $F_L(F_R)$ represents the ocean-generated force on the left (right) side of the continental Plate A, while F_L'(F_R') and F_L''(F_R'') denote the horizontal and vertical forces decomposed from the ocean-generated force, respectively. Given Plate A moves towards the right (marked with blue arrow), the term f_{base} denotes the basal friction force exerted by the underlying asthenosphere, while f_{right}, f_{far}, and f_{near} denote the collisional force from Plate C on the right side, the shearing force from the plate on the far side, and the shearing force from the plate on the near side of Plate A, respectively. L denotes the width of the continent's side; h_L and h_R are the ocean's depth on the left and right, respectively. α and β denote the inclinations of the continent's slope on either side. Note that the ocean depth and the lithospheric plate's thickness are highly exaggerated.

3.1.2 Continental plate's motion

Equation (1) provides three possibilities for the continental plate. If the final horizontal force is greater than the total resistive force, the combined force is greater than zero, and the continental plate would be subjected to an accelerating motion. Practically, it is impossible for the continental plate to undergo such a movement. If the final horizontal force is equal to the total resistive force, the combined force is zero, and the continental plate would be subjected to a steady motion. If the final horizontal force is less than the total resistive force, the combined force is less than zero, and the continental plate would remain motionless. The resistive forces, as shown in Figure 3, include three parts: the friction force at the base, the collisional force at the front, and the shearing forces at the near and far sides. Such a force distribution would require the adjacent plates to move entirely parallel to the sample plate. This cannot be realistic because the movements of most of plates are intersecting with each other. For instance, the South American Plate moves north-westward, the Nazca Plate moves eastward; The African Plate moves north-eastward, the Eurasian Plate rotates clockwise. These nonparallel movements would yield additional collisional force and shearing force. Here, we assume these additional forces yield a latitudinal component, this latitudinal component further combines the final horizontal force to form a net force. The net force finally determines the movement of the sample plate. We then divide the net force into two parts to exert: one, as an opposing force, balances the collisional force at the front and the shearing forces at the near and far sides, and the other, as a driving force, balances the basal

friction force. With an assumption that the acceleration and inertia of plate are neglected, these balances of forces allow the plate's motion to be steadily maintained. The balance between the driving force and the basal friction force may be written as

$$F_{driving} - f_{basal} = 0 \quad (2)$$

where $F_{driving}$ denotes the driving force and f_{basal} denotes the basal friction force. The basal friction force exerted by the asthenosphere along the plate's base can be expressed as $f_{basal} = \mu Au/y$, where μ, A, u, and y are the viscosity of the asthenosphere, the plate's area, the plate's speed, and the thickness of the asthenosphere, respectively. In practice, the continent's side is not flat, and the continent's base is generally wider than its top, making the continent look more like a circular truncated cone standing in the ocean. As the horizontal force generated is related to the ocean's width (i.e., the continent side's width), we need to horizontally project the continent into a polygonal column, dissect the whole side of this column into a series of smaller rectangular sides connecting one to another and subsequently calculate the horizontal force generated at each of these rectangular sides. Here, four continental plates (South American, African, Indian, and Australian) are selected to demonstrate the horizontal forces and resultant movements (Figure 4). The longitude and latitude of the control sites (e.g., numbers 1, 2, 3, ...) determine the lengths of the continent's sides.

As the horizontal forces exerted on the continent's sides are often along different directions and the Earth's surface is curved, these vector forces need to be combined together. To facilitate the following deduction, we employ a three-dimensional coordinate system and decompose each of the horizontal forces into three forces along the *x*, *y*, and *z* axis (Figure 5). Subsequently, by simple addition, all of the *x*, *y*, and *z* axis forces are separately combined into a total *x* axis force, total *y* axis force, and total *z* axis force. We further assume that each of these three total forces is exerted on the continent's geometric center, from where the total *x* axis force yields a latitudinal force, the total *y* axis force also yields a latitudinal force, and the total *z* axis force yields a longitudinal force. A simple addition of these two latitudinal forces represents a total latitudinal force, then, a combination of the total latitudinal force and the longitudinal force represents the final horizontal force. The final horizontal force may be written as $F_{final}=(F_{latitudinal}^2+F_{longitudinal}^2)^{0.5}$, where $F_{latitudinal}$ and $F_{longitudinal}$ are the total latitudinal force and the longitudinal force, respectively. The total latitudinal and the longitudinal forces can be expressed as $F_{latitudinal}=-F_x\sin\sigma+F_y\cos\sigma$, $F_{longitudinal}=F_z\cos\varphi$, where F_x, F_y, and F_z denote the total *x*, *y*, and *z* axis force,

respectively. These forces can be expressed as $F_x = \sum_{i=1}^{n} F_{i-x}$, $F_y = \sum_{i=1}^{n} F_{i-y}$, and $F_z = \sum_{i=1}^{n} F_{i-z}$, where $F_{i\text{-}x}$, $F_{i\text{-}y}$, and $F_{i\text{-}z}$ denote the x, y, and z axis force that are decomposed from the horizontal force generated at the ith side of the continent, $F_{i\text{-}x}$= -F_i(sin$\gamma_i$sin$\beta_i$cosα_i+cos$\gamma_i$sinα_i), $F_{i\text{-}y}$= F_i (cos$\gamma_i$cosα_i-sin$\gamma_i$sin$\beta_i$sinα_i), and $F_{i\text{-}z}$= F_i sin$\gamma_i$cosβ_i. α_i and β_i denote the longitude and latitude of the hypothetical center of geometry of the ith side, on which the horizontal force F_i is exerted. They may be approximately represented by an average of the longitude and latitude of the two sites that are located at the two ends of the side, and can be written as α_i=(d_M+d_N)/2 and β_i=(q_M+q_N)/2, where d_M, d_N, q_M, and q_N denote the longitude and latitude of the two sites. γ_i denotes the inclination of the horizontal force F_i to the latitudinal direction and can be obtained through the longitude and latitude of the two sites at the side. The horizontal force F_i may be written as F_i=0.5ρg$L_i h_{i\text{-ocean}}^2$, and ρ, g, L_i, and $h_{i\text{-ocean}}$ are the density of water, gravitational acceleration, length of the ith side, and the ocean depth that connects to the ith side. σ and φ denote the longitude and latitude of the hypothetical center of geometry of the continent, they may be approximately represented with the mean longitude and latitude of all the control sites on the continent and can be written as $\sigma = \sum_{j=1}^{n} d_j / n$, and $\varphi = \sum_{j=1}^{n} q_j / n$, where d_j and q_j denote the longitude and latitude of the jth site, and n denotes the total number of sites. The parameters involved for the four selected plates and final calculated horizontal forces are separately listed in Tables 1 and 2.

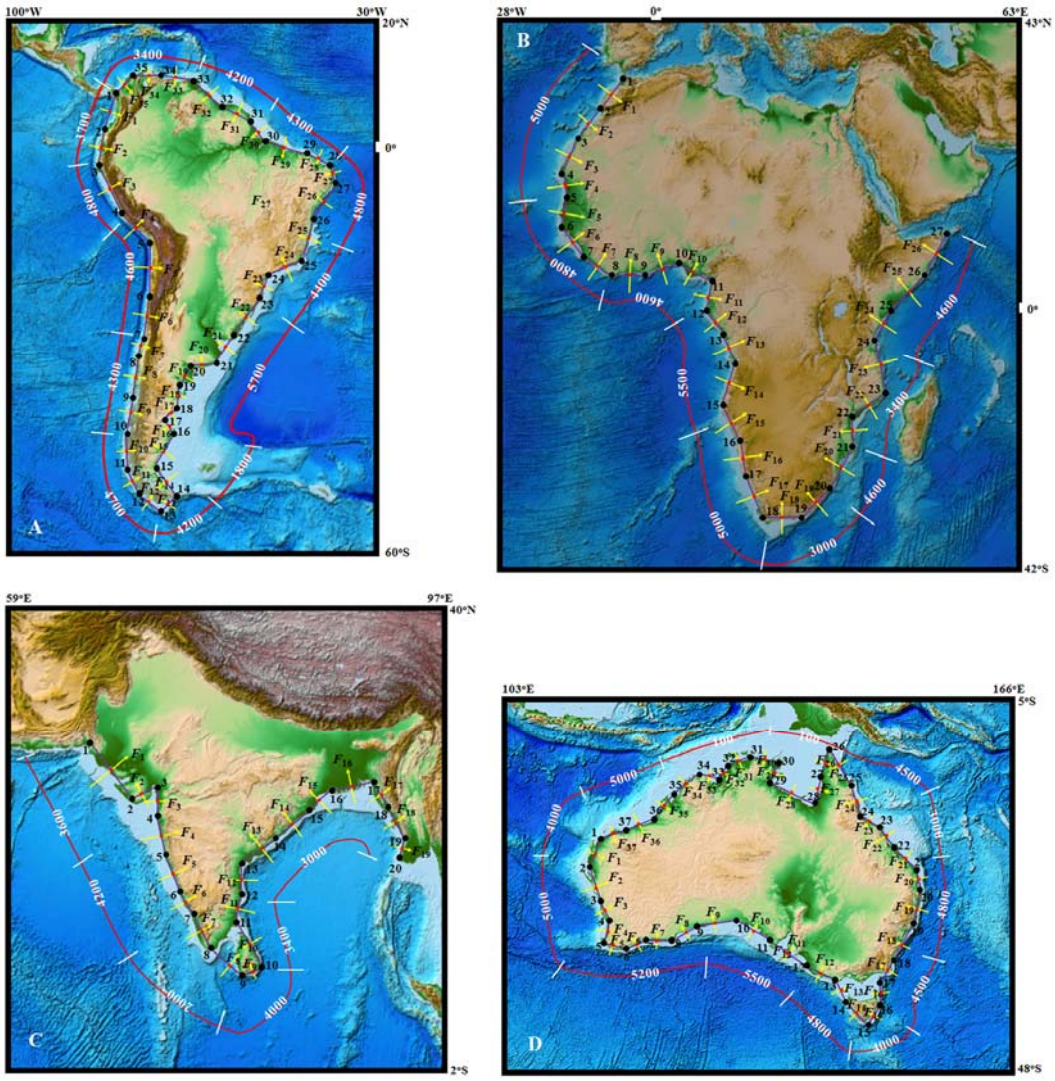

Figure 4. Geographic treatment of the control sites for the four selected continental plates and the horizontal forces generated for them. *F* (yellow arrows) denotes the generated horizontal force, while the purple bars denote the distances affected by the horizontal forces. The product of this distance and ocean depth is the area to which the horizontal force is applied. The red lines depict the ocean depths (marked with white number) that are used to calculate the horizontal forces. The black dots with numbers denote the control sites; the red dots in the purple bars denote the hypothetical centers of geometry of the sides. The background map was made through the ETOPO1 Global Relief Model (Amante and Eakins, 2009)**.** Note that the ocean depths were artificially resolved through Bathymetric Data Viewer of NOAA.

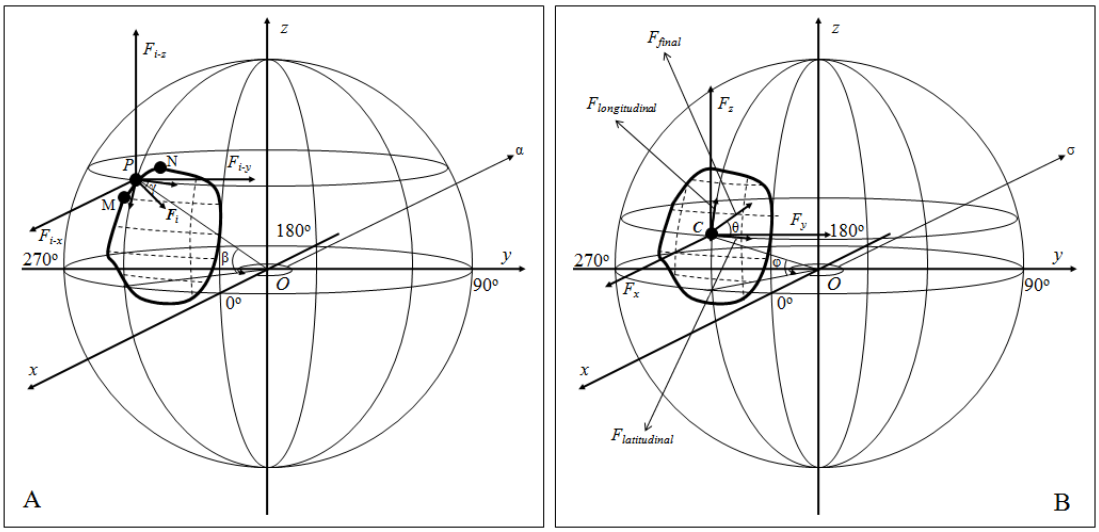

Figure 5. Modeling the vector force along the Earth's curved surface. (A) The horizontal force F_i is decomposed into the *x* axis force $F_{i\text{-}x}$, *y* axis force $F_{i\text{-}y}$, and *z* axis force $F_{i\text{-}z}$. Site *P* denotes the hypothetical center of geometry of the *i*th side (line *MN*, for instance) of a continent, on which the horizontal force F_i is exerted. α and β denote the longitude and latitude of the hypothetical center of geometry of the *i*th side. γ denotes the inclination of the horizontal force F_i to the latitudinal direction. **(B) The total *x* axis force F_x, total *y* axis force F_y, and total *z* axis force F_z are combined into a final horizontal force F_{final}.** $F_{latitudinal}$ and $F_{longitudinal}$ denote the latitudinal force and longitudinal force, respectively. Site *C* denotes the hypothetical center of geometry of the continent. σ and φ denote the longitude and latitude of the hypothetical center of geometry, and θ denotes the inclination of the final force F_{final} to the latitudinal direction.

Table 1(A). Basic information for the selected four continental plates

Plate	Area	Control site		Hypothetical geometric center of the continent			Side			Ocean depth
							Length	Hypothetical geocentric center of the side		
	S		d_j	q_j	σ	φ	i	L_i	α_i	β_i	$h_{i\text{-ocean}}$
	km^2	j	Longitude(^{o})	Latitude(^{o})	Longitude(^{o})	Latitude(^{o})		km	Longitude(^{o})	Latitude(^{o})	m
South America	43,600,000	1	282.76	7.68			1	816.09	281.29	4.32	3,700
		2	279.81	0.95			2	722.12	279.57	-2.29	3,700
		3	279.32	-5.53			3	1100.61	281.57	-9.96	4,800
		4	283.82	-14.39			4	785.36	286.64	-16.68	4,600
		5	289.45	-18.96			5	947.21	289.31	-23.22	4,600

6	289.16	-27.48		6	544.94	288.88	-29.92	4,600
7	288.60	-32.36		7	411.83	287.83	-34.10	4,300
8	287.06	-35.84		8	827.79	286.36	-39.53	4,300
9	285.65	-43.21		9	541.09	285.16	-45.62	4,300
10	284.66	-48.03		10	402.38	284.73	-49.84	4,700
11	284.80	-51.65		11	361.74	285.93	-53.13	4,700
12	287.06	-54.61		12	313.26	288.96	-55.53	4,700
13	290.85	-56.44		13	306.62	292.68	-55.53	4,200
14	294.50	-54.61		14	364.95	292.75	-53.35	5,500
15	290.99	-52.08		15	571.30	292.40	-49.68	1,800
16	293.80	-47.27		16	202.81	293.10	-46.50	5,700
17	292.40	-45.72		17	226.69	293.39	-44.98	1,800
18	294.37	-44.23		18	365.58	294.86	-42.63	5,700
19	295.35	-41.02		19	339.61	296.41	-39.73	5,700
20	297.46	-38.43		20	418.60	299.85	-38.27	4,200
21	302.24	-38.10		21	558.42	304.14	-36.11	5,700
22	306.04	-34.12		22	800.29	308.36	-31.12	5,700

22					22				
23	310.68	-28.11			23	534.12	311.88	-25.96	4,400
24	313.07	-23.81			24	589.13	315.75	-22.84	4,400
25	318.42	-21.86			25	810.47	319.83	-18.47	4,400
26	321.23	-15.07			26	889.55	323.20	-11.56	4,800
27	325.16	-8.05			27	433.76	324.67	-6.16	4,800
28	324.18	-4.27			28	608.35	321.65	-3.22	4,300
29	319.12	-2.16			29	840.78	315.47	-1.18	4,300
30	311.81	-0.20			30	416.41	310.41	1.04	4,300
31	309.00	2.28			31	717.41	306.26	3.99	4,200
32	303.51	5.70			32	778.80	300.84	8.00	4,200
33	298.16	10.29			33	743.58	294.79	10.78	3,400
34	291.42	11.26			34	552.89	288.89	11.19	3,400
35	286.35	11.12	297.49	-23.95	35	96.18	284.56	9.40	3,400

Notes: all geographic sites refer to Figure 4. The negative symbol "-" for latitude denotes south of equator.

Table 1(B). (continue) Basic information for the selected four continental plates

Plate	Area	Control site		Hypothetical geometric center of the continent		Side				Ocean depth
							Length	Hypothetical geocentric center of the side		
	S	j	d_j	q_j	σ	φ	i	L_i	α_i	β_i	$h_{i\text{-ocean}}$
	km^2		Longitude(^{o})	Latitude(^{o})	Longitude(^{o})	Latitude(^{o})		km	Longitude(^{o})	Latitude(^{o})	m
Africa	61,300,000	1	354.42	35.07			1	603.37	352.31	33.01	5,000
		2	350.20	30.95			2	580.67	348.16	29.04	5,000
		3	346.12	27.13			3	680.56	344.64	24.38	5,000
		4	343.16	21.63			4	460.59	343.45	19.58	5,000
		5	343.73	17.52			5	515.90	343.45	15.22	4,800
		6	343.16	12.91			6	744.56	345.27	10.28	4,800
		7	347.38	7.65			7	599.29	349.61	6.12	4,600
		8	351.84	4.58			8	721.61	355.10	4.72	4,600
		9	358.35	4.86			9	643.53	1.06	5.63	4,600
		10	3.96	6.40			10	663.57	6.71	5.21	4,600
		11	9.46	4.02			11	565.35	9.32	1.48	4,600
		12	9.18	-1.06			12	629.29	10.73	-3.44	5,500
		13	12.27	-5.81			13	500.33	13.12	-7.90	5,500
		14	13.96	-9.99			14	835.05	12.91	-13.61	5,500
		15	11.85	-17.22			15	690.91	13.19	-20.07	5,200
		16	14.52	-22.91			16	709.88	15.65	-25.94	5,000
		17	16.77	-28.97			17	638.10	18.11	-31.61	5,000
		18	19.45	-34.24			18	599.91	22.69	-33.95	3,000
		19	25.92	-33.65			19	667.90	28.45	-31.56	3,000

	20	30.98	-29.46			20	861.11	33.16	-26.12	4,600
	21	35.34	-22.77			21	528.53	35.55	-20.40	3,400
	22	35.76	-18.03			22	598.23	38.15	-16.62	3,400
	23	40.54	-15.20			23	1038.15	39.49	-10.65	3,800
	24	38.43	-6.09			24	787.89	40.40	-3.14	4,600
	25	42.37	-0.19			25	762.31	44.97	2.05	4,600
	26	47.57	4.29			26	955.79	49.68	8.05	4,600
	27	51.79	11.81	13.28	-2.10					

Notes: all geographic sites refer to Figure 4. The negative symbol "-" for latitude denotes south of equator.

Table 1(C). (continue) Basic information for the selected four continental plates

Plate	Area	Control site		Hypothetical geometric center of the continent		Side				Ocean depth
						i	Length	Hypothetical geocentric center of the side		
	S	j	d_j	q_j	σ	φ	L_i	α_i	β_i	$h_{i\text{-ocean}}$
	km^2		Longitude(^{o})	Latitude(^{o})	Longitude(^{o})	Latitude(^{o})	km	Longitude(^{o})	Latitude(^{o})	m
India	11,900,000	1	66.71	25.68			1	653.96	68.61	23.31	3,600
		2	70.51	20.94			2	243.27	71.55	21.46	4,000
		3	72.58	21.98			3	229.37	72.65	20.95	3,600
		4	72.72	19.92			4	374.54	73.06	18.27	3,600
		5	73.39	16.61			5	381.51	74.17	15.07	4,200
		6	74.94	13.52			6	271.02	75.52	12.44	4,200
		7	76.10	11.36			7	374.65	76.84	9.84	2,000
		8	77.58	8.32			8	402.32	78.99	7.17	2,000

	9	80.39	6.01			9	186.08	81.11	6.45	4,000
	10	81.83	6.88			10	482.71	80.70	8.74	3,400
	11	79.56	10.60			11	269.68	79.94	11.76	3,400
	12	80.32	12.91			12	322.27	80.34	14.36	3,000
	13	80.35	15.81			13	385.87	81.78	16.89	3,000
	14	83.20	17.96			14	444.56	84.93	19.12	3,000
	15	86.65	20.28			15	232.97	87.35	21.10	3,000
	16	88.05	21.92			16	391.64	89.93	22.20	3,000
	17	91.81	22.47			17	273.00	92.38	21.36	3,000
	18	92.94	20.25			18	334.21	93.80	18.99	3,000
	19	94.66	17.72			19	185.47	94.43	16.92	3,000
	20	94.20	16.11	80.92	16.36					

Notes: all geographic sites refer to Figure 4.

Table 1(D). (continue) Basic information for the selected four continental plates

Plate	Area	Control site				Hypothetical geometric center of the continent		Side				Ocean depth
								i	Length	Hypothetical geocentric center of the side		
	S	j	d_j	q_j	σ	φ			L_i	α_i	β_i	$h_{i\text{-ocean}}$
	km^2		Longitude(^{o})	Latitude(^{o})	Longitude(^{o})	Latitude(^{o})			km	Longitude(^{o})	Latitude(^{o})	m
Australia	47,000,000	1	114.49	-21.83				1	356.76	114.04	-23.38	4,000
		2	113.58	-24.93				2	492.15	114.28	-27.06	5,000
		3	114.98	-29.18				3	299.49	115.37	-30.49	5,000
		4	115.76	-31.79				4	268.95	115.44	-32.97	5,000
		5	115.12	-34.15				5	303.60	116.67	-34.64	5,200
		6	118.22	-35.13				6	241.34	119.20	-34.41	5,200

7	120.18	-33.68	7	312.71	121.87	-33.65	5,200
8	123.56	-33.62	8	316.31	124.97	-32.83	5,200
9	126.37	-32.03	9	482.81	128.90	-31.73	5,500
10	131.43	-31.43	10	455.55	133.37	-32.68	5,500
11	135.30	-33.92	11	523.56	137.52	-35.44	5,500
12	139.73	-36.95	12	398.28	141.70	-37.84	4,800
13	143.67	-38.73	13	325.98	144.13	-40.16	4,800
14	144.58	-41.58	14	332.23	146.02	-42.64	4,800
15	147.46	-43.69	15	256.24	147.99	-42.61	4,000
16	148.52	-41.52	16	280.09	148.56	-40.26	4,500
17	148.59	-39.00	17	346.31	149.40	-37.58	4,500
18	150.21	-36.16	18	551.52	151.41	-33.89	4,600
19	152.60	-31.61	19	419.94	152.95	-29.75	4,800
20	153.30	-27.88	20	340.18	153.02	-26.37	4,800
21	152.74	-24.86	21	359.55	151.58	-23.64	3,000
22	150.42	-22.42	22	324.49	149.37	-21.34	3,000
23	148.31	-20.26	23	287.94	147.26	-19.43	4,500
24	146.20	-18.60	24	339.19	145.81	-17.12	4,500
25	145.42	-15.64	25	620.53	143.95	-13.25	4,500
26	142.47	-10.85	26	423.89	142.02	-12.71	100
27	141.56	-14.56	27	311.39	141.17	-15.91	100
28	140.78	-17.26	28	648.16	137.99	-16.11	100
29	135.20	-14.96	29	320.61	135.78	-13.63	100
30	136.35	-12.30	30	429.74	134.42	-11.89	100
31	132.49	-11.47	31	288.53	131.37	-12.16	100
32	130.24	-12.85	32	231.21	129.82	-13.81	100
33	129.39	-14.76	33	308.34	128.09	-14.18	100

	34	126.79	-13.60			34	427.24	125.32	-14.89	100
	35	123.84	-16.18			35	423.32	122.58	-17.66	5,000
	36	121.31	-19.13			36	361.49	119.73	-19.79	5,000
	37	118.15	-20.45	134.58	-25.92	37	409.14	116.32	-21.14	5,000

Notes: all geographic sites refer to Figure 4. The negative symbol "-" for latitude denotes south of equator.

Table 2(A). The ocean-generated force for the selected four plates

Plate	i	horizontal		decomposed			$F_{latitudinal}$	$F_{longitudinal}$	F_{final}
		F_i	Inclination to latitude, east (γ_i)	$F_{i\text{-}x}$	$F_{i\text{-}y}$	$F_{i\text{-}z}$			
		N ($*10^{17}$)	Degrees (^{o})				N ($*10^{17}$)		
South America	1	0.5474	336.33	0.4949	0.0819	-0.2192			
	2	0.4844	355.68	0.4761	0.0817	-0.0365			
	3	1.2425	26.93	1.1048	0.1269	0.5542			
	4	0.8143	50.93	0.5436	-0.0269	0.6056			
	5	0.9821	358.05	0.9220	0.3369	-0.0307			
	6	0.5650	353.45	0.5207	0.2120	-0.0558			
	7	0.3731	336.13	0.2989	0.1851	-0.1250			
	8	0.7500	349.17	0.6816	0.2935	-0.1087			
	9	0.4902	348.39	0.4451	0.1936	-0.0690			
	10	0.4355	2.21	0.4242	0.0982	0.0109			
	11	0.3916	37.36	0.3514	-0.0974	0.1426			
	12	0.3391	64.23	0.2212	-0.1902	0.1728			
	13	0.2650	116.63	-0.0343	-0.2260	0.1341			

	14	0.5409	234.22	-0.4278	0.2024	-0.2620			
	15	0.0907	149.71	-0.0591	-0.0621	0.0296			
	16	0.3229	222.09	-0.2820	0.0504	-0.1490			
	17	0.0360	127.10	-0.0119	-0.0272	0.0203			
	18	0.5820	163.02	-0.4567	-0.3384	0.1250			
	19	0.5407	140.83	-0.2784	-0.3819	0.2626			
	20	0.3618	93.95	0.0897	-0.2063	0.2834			
	21	0.8890	136.33	-0.3291	-0.6603	0.4960			
	22	1.2741	142.33	-0.5411	-0.9414	0.6666			
	23	0.5067	150.93	-0.2578	-0.3759	0.2213			
	24	0.5589	110.03	0.0124	-0.2793	0.4839			
	25	0.7688	157.52	-0.3872	-0.6029	0.2789			
	26	1.0043	150.76	-0.4463	-0.7605	0.4806			
	27	0.4897	194.53	-0.2849	-0.3791	-0.1222			
	28	0.5512	247.36	-0.1540	-0.1487	-0.5079			
	29	0.7618	254.99	-0.1492	-0.1300	-0.7356			
	30	0.3773	228.57	-0.1868	-0.1657	-0.2828			
	31	0.6201	238.08	-0.2427	-0.2234	-0.5251			
	32	0.6732	229.37	-0.3399	-0.2857	-0.5059			
	33	0.4212	261.81	-0.0218	-0.0959	-0.4095			
	34	0.3132	268.42	0.0115	-0.0603	-0.3071			
	35	0.0545	313.78	0.0381	0.0033	-0.0388			
				1.7453	-4.7996	0.4776	-0.6675	0.4365	0.7976

Note: all related forces refer to Figure 4 and Figure 5.

Table 2(B). (continue) The ocean-generated force for selected four plates

Plate	i	horizontal		decomposed			$F_{latitudinal}$	$F_{longitudinal}$	F_{final}
		F_i	Inclination to latitude, east (γi)	F_{i-x}	F_{i-y}	F_{i-z}			
		N (*10^{17})	Degrees (^{o})	N (*10^{17})					
Africa	1	0.7391	314.31	0.3546	0.4731	-0.4435			
	2	0.7113	313.11	0.3464	0.4241	-0.4540			
	3	0.8337	331.71	0.3517	0.6647	-0.3599			
	4	0.5642	7.90	0.1344	0.5431	0.0730			
	5	0.5824	352.95	0.1827	0.5487	-0.0690			
	6	0.8406	38.74	0.0759	0.6580	0.5176			
	7	0.6214	55.46	0.0099	0.3564	0.5089			
	8	0.7482	87.54	-0.0585	0.0373	0.7450			
	9	0.6672	105.35	-0.0598	-0.1778	0.6403			
	10	0.6880	66.60	-0.0889	0.2647	0.6288			
	11	0.5862	356.85	-0.0940	0.5777	-0.0322			
	12	0.9328	33.05	-0.1156	0.7739	0.5077			
	13	0.7416	22.01	-0.1188	0.6783	0.2753			
	14	1.2378	343.73	-0.3449	1.1400	-0.3370			
	15	0.9154	25.14	-0.0591	0.8373	0.3653			
	16	0.8696	20.37	-0.0923	0.8207	0.2722			
	17	0.7817	26.96	-0.0401	0.7200	0.3018			
	18	0.2646	84.79	0.1265	0.0789	0.2186			
	19	0.2945	129.63	0.1939	-0.1086	0.1933			
	20	0.8928	146.91	0.5888	-0.5088	0.4377			
	21	0.2994	174.94	0.1809	-0.2373	0.0248			
	22	0.3389	120.63	0.1722	-0.0843	0.2794			
	23	0.7346	193.04	0.4314	-0.5718	-0.1629			

	24	0.8169	146.27	0.4592	-0.5013	0.4530			
	25	0.7904	130.75	0.3494	-0.3801	0.5984			
	26	0.9910	150.70	0.6150	-0.6110	0.4802			
				3.5009	6.4160	5.6629	5.4404	5.6591	7.8501

Note: all related forces refer to Figure 4 and Figure 5.

Table 2(C). (continue) The ocean-generated force for the selected four plates

Plate	i	horizontal		decomposed			$F_{latitudinal}$	$F_{longitudinal}$	F_{final}
		F_i	Inclination to latitude, east (γ_i)	$F_{i\text{-}x}$	$F_{i\text{-}y}$	$F_{i\text{-}z}$			
		N ($*10^{17}$)	Degrees (^{o})				N ($*10^{17}$)		
India	1	0.4153	38.72	-0.3392	0.0225	0.2386			
	2	0.1907	116.68	0.0615	-0.0862	0.1586			
	3	0.1457	3.89	-0.1398	0.0400	0.0092			
	4	0.2378	11.44	-0.2273	0.0538	0.0448			
	5	0.3298	26.64	-0.2941	0.0435	0.1428			
	6	0.2343	28.24	-0.2058	0.0285	0.1082			
	7	0.0734	25.96	-0.0655	0.0097	0.0317			
	8	0.0789	50.58	-0.0506	0.0021	0.0604			
	9	0.1459	121.14	0.0724	-0.0255	0.1241			
	10	0.2734	211.39	0.2338	-0.0164	-0.1408			
	11	0.1528	161.79	0.1412	-0.0349	0.0467			
	12	0.1421	179.41	0.1400	-0.0242	0.0014			
	13	0.1702	127.03	0.0958	-0.0537	0.1300			
	14	0.1961	123.92	0.1043	-0.0628	0.1537			
	15	0.1027	139.51	0.0769	-0.0276	0.0622			

	16	0.1727	98.32	0.0249	-0.0646	0.1582			
	17	0.1204	26.98	-0.1064	-0.0243	0.0509			
	18	0.1474	34.21	-0.1198	-0.0350	0.0784			
	19	0.0818	344.05	-0.0789	0.0004	-0.0215			
				-0.6766	-0.2548	1.4377	0.6279	1.3795	1.5156

Note: all related forces refer to Figure 4 and Figure 5.

Table 2(D). (continue) The ocean-generated force for the selected four plates

Plate	i	horizontal		decomposed			$F_{latitudinal}$	$F_{longitudinal}$	F_{final}
		F_i	Inclination to latitude, east (γ_i)	$F_{i\text{-}x}$	$F_{i\text{-}y}$	$F_{i\text{-}z}$			
		N (*10^{17})	Degrees (^{o})	N (*10^{17})					
Australia	1	0.2797	343.64	-0.2324	-0.1379	-0.0723			
	2	0.6029	18.23	-0.5572	-0.1573	0.1680			
	3	0.3669	16.64	-0.3404	-0.1025	0.0905			
	4	0.3295	344.83	-0.2670	-0.1790	-0.0723			
	5	0.4023	72.46	-0.2062	0.1404	0.3156			
	6	0.3198	126.49	0.0951	0.2196	0.2121			
	7	0.4143	91.02	-0.1150	0.1988	0.3449			
	8	0.4191	119.50	0.0558	0.2803	0.3065			
	9	0.7156	96.76	-0.1691	0.3438	0.6044			
	10	0.6752	57.24	-0.4761	-0.0280	0.4780			
	11	0.7760	55.63	-0.5698	-0.0723	0.5219			
	12	0.4496	65.69	-0.3120	0.0105	0.3236			
	13	0.3680	17.71	-0.2639	-0.2418	0.0856			
	14	0.3751	53.77	-0.2938	-0.0693	0.2226			

	15	0.2009	153.97	0.0451	0.1847	0.0649		
	16	0.2779	178.41	0.1407	0.2396	0.0059		
	17	0.3436	150.30	0.0626	0.3098	0.1349		
	18	0.5718	152.29	0.1121	0.5155	0.2208		
	19	0.4741	169.37	0.1733	0.4347	0.0759		
	20	0.3841	190.51	0.1990	0.3224	-0.0627		
	21	0.1586	223.56	0.0932	0.0802	-0.1001		
	22	0.1431	224.33	0.0835	0.0695	-0.0931		
	23	0.2857	231.81	0.1584	0.1082	-0.2118		
	24	0.3366	194.76	0.2038	0.2550	-0.0820		
	25	0.6157	211.63	0.3684	0.3803	-0.3143		
	26	0.0002	346.22	-0.0001	-0.0002	0.0000		
	27	0.0002	343.89	-0.0001	-0.0001	0.0000		
	28	0.0003	247.60	0.0001	0.0000	-0.0003		
	29	0.0002	156.62	0.0001	0.0001	0.0001		
	30	0.0002	257.86	0.0001	0.0000	-0.0002		
	31	0.0001	301.52	0.0000	-0.0001	-0.0001		
	32	0.0001	336.01	-0.0001	-0.0001	0.0000		
	33	0.0002	245.96	0.0001	0.0000	-0.0001		
	34	0.0002	311.17	-0.0001	-0.0001	-0.0002		
	35	0.5186	319.38	-0.2766	-0.2982	-0.3217		
	36	0.4428	292.67	-0.0796	-0.2048	-0.3845		
	37	0.5012	290.66	-0.0835	-0.2300	-0.4374		
				-2.4518	2.3721	2.0229	0.0816	1.8194	1.8212

Note: all related forces refer to Figure 4 and Figure 5.

The asthenosphere viscosity is not exactly determined. Many numerical studies using glacial isostatic adjustment and geoid modeling showed that the asthenospheric viscosity ranges from 10^{17} to 10^{20} Pa s (e.g., Steinberger, 2016; Hager and Richards, 1989; Mitrovica, 1996; King, 1995; Kido et al., 1998; James et al., 2009; Pollitz et al., 1998; Berker, 2017; Kaufmann and Lambeck, 2000; Hu et al., 2016). Laboratory experiments, however, suggested that the magnitude of the asthenosphere viscosity could be substantially different from those constrained from numerical studies. The viscosity is variable and likely related to the thermodynamic state, grain size, composition of the medium, and state of stress (Bercovici et al., 2015). Both the melt contents of asthenosphere and the water in the asthenosphere may greatly affect the viscosity (Mei et al., 2002; Hirth and Kohlstedt, 1996). Hirth and Kohlstedt (1996) reported a variable viscosity profile for a melt-free oceanic lithosphere, the mean value of this viscosity profile is ~10^{18} Pa s. These authors (e.g., Doglioni et al., 2011; Scoppola et al., 2006) concluded that, in consideration of the water- and melt-rich layers characterized by much lower viscosities, a strong vertical variability of viscosity may be more realistic. The asthenosphere's effective viscosity can be greatly lowered to 10^{15} Pa s if water content in the case of both diffusion and dislocation creeps is included (Korenaga and Karato, 2008). Scoppola et al. (2006) made a more detailed review of the asthenosphere viscosity, and concluded that the presently accepted values of viscosity might be reduced through a combined experiment including these parameters (i.e., melt content, water content, mechanical asnisotropy, and shear localization). A "superweak", low-viscosity asthenosphere supported by recent obsevations is being accepted by geophysical community (Kawakatsu et al., 2009; Hawley et al., 2016; Holtzman, 2016; Naif et al., 2013; Freed et al., 2017; Hu et al., 2016; Stern et al., 2015; Bercker, 2017). Jordan (1974) treated the asthenospheric thickness as 300 km.

Taking into account the present status of the viscosity and thickness of the asthenosphere above, we adopt y=300 km for each of the selected four plates, $\mu=10^{18}$ Pa s for the South American, African, and Indian plates, and $\mu=0.6\times10^{18}$ Pa s for the Australian Plate. We term the latitudinal component, which is yielded by these additional collisional and shearing forces, as $F_{latitudinal\text{-}additional}$, and assume its magnitude to be 75%, 10%, 45%, and 52% of the final horizontal force respectively for the South American, African, Indian, and Australian plates; We term the net force, which is a combination of the latitudinal component and the final horizontal force, as

F_{net}, and assume 95%, 25%, 50%, and 95% of this force to be used acting as the driving force $F_{driving}$ respectively for the South American, African, Indian, and Australian plates. Taking the plate's area in Table 1 and the final horizontal force F_{final} in Table 2, we use equation (2) to resolve the continental plate's speed, i.e., $u= F_{driving} y/\mu A$. The movement's orientation is determined by the direction of the net force and may be expressed as $\Delta\theta=\theta-\theta_1$, where $\tan\theta = F_{longitudinal}/F_{latitudinal}$, and $\cos\theta_1=(F_{final}^2+F_{net}^2- F_{latitudinal\text{-}adjacent}^2)/2F_{final} F_{net}$. The related forces and calculated movements for these plates are listed in Table 3.

The above treatment of the continental plate's motion is rather idealized. Because most of the horizontal forces exerted on the continental plate cannot intersect with each other, this may produce a torque effect to rotate the continental plate. Figures 6 (A and B) conceptually demonstrate how these continental plates (North American and Eurasian, for example) move under the torque produced by the horizontal forces. A more detailed description about this torque effect will be shown in another work.

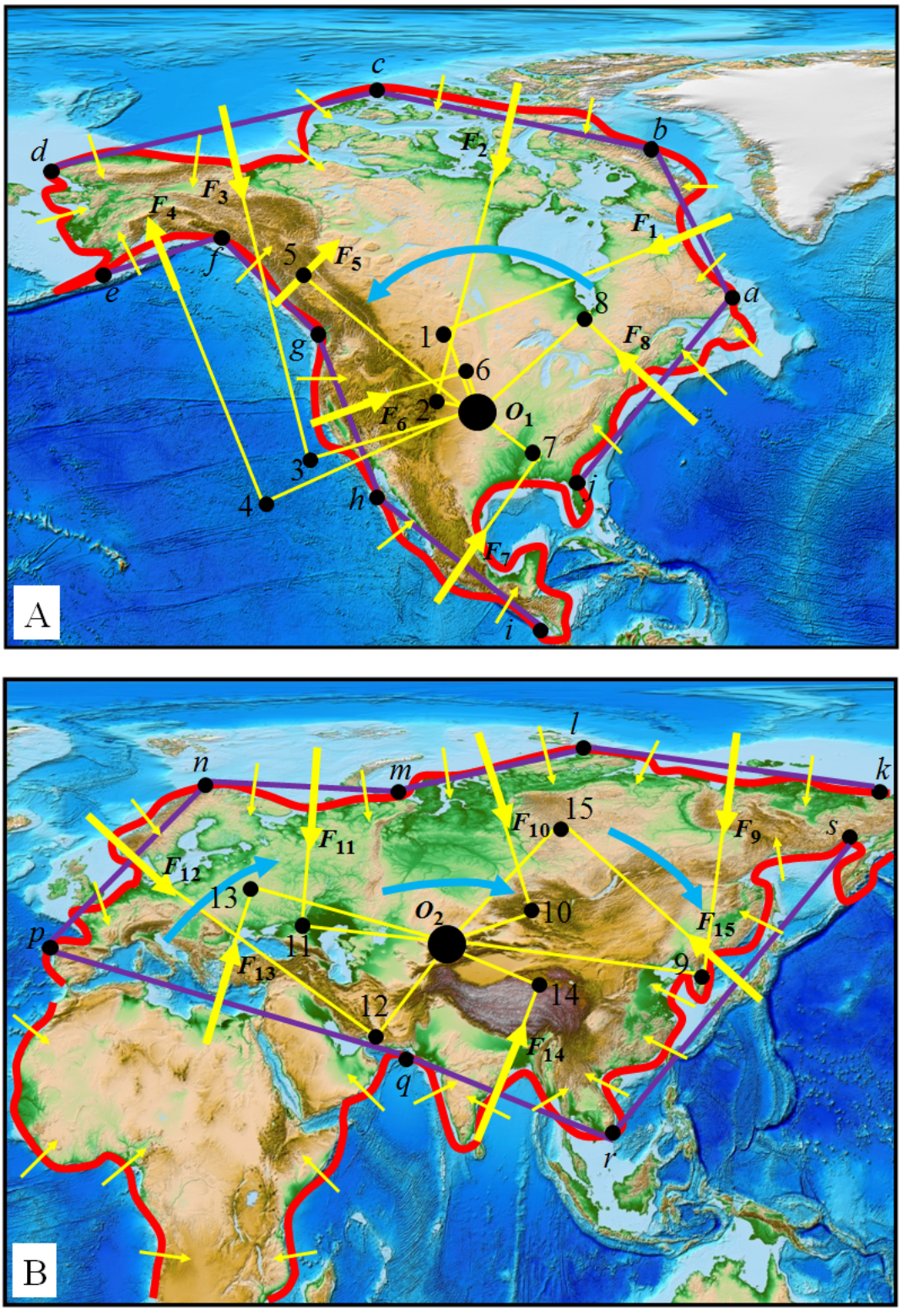

Figure 6. Dynamics for the rotation of the Eurasian and North American plates. O_1 and O_2 denote possible positions of the barycenters of the two plates. F_1, F_2, and F_3,

i.e., marked with yellow arrows, denote the horizontal forces generated; *a*, *b*, and *c*, i.e., denote the selected control sites, while *ab*, *bc*, and *cd*, i.e., marked with purple bars, denote the lengths of the continents' sides; and $O_1 1$, $O_1 2$,. ..,$O_2 9$, and $O_2 10$ denote the arms to which the horizontal forces are applied. The torque effect is a product of the force and arm. Curved blue arrows represent expected rotations around these barycenters. It should be noted that F_{13} represents a lateral push force from the traveling Africa Plate. The background map was made through the ETOPO1 Global Relief Model (Amante and Eakins, 2009).

3.1.3 Oceanic plate's motion

As mentioned earlier, a portion of the net force is used to oppose the collisional and shearing forces from the adjacent plates. According to the principle of action and reaction, the net force pushes/shears the adjacent plates.

The oceanic plate's motion can be realized by the force that transfers from the continental plate to the oceanic plate. This tranferring of force may be exemplified by the Pacific plate's motion. As outlined in Figure 7, we assume, by means of a force vector, that the North American plate provides a push force F_{PN} on the hypothetical center of geometry of the Pacific plate, and that the Australian plate provides a push force F_{PA} on the hypothetical center of geometry. The combination of these two forces is the final horizontal force F_P, which contributes to the dynamics of the Pacific plate. The other forces that act on the Pacific plate include the collisional force from the part of North American Plate and the Eurasian Plate, the basal friction force exerted by the underlying asthenosphere, the shearing force from the Australian plate, and the shearing force from the North American plate. These other forces are denoted F_{far}, f_{base}, F_{right}, and F_{left} , respectively. As mentioned in section 3.1, we assume f_{base} to be a resistive force. And then, we separate the final horizontal force into two parts to exert: one, as an opposing force, balances the collisional force and shearing forces, and the other, as a driving force, balances the basal friction force. These balances of forces allow this plate's motion to be steadily maintained under the assumption that the acceleration and inertia of plate is neglected. Both the North and South American continents are located between the Atlantic Ocean and the Pacific Ocean, the coastline of the North American continent is longer than that of the South American continent, and the two continents have greater longitudinal than latitudinal extents. The final horizontal force for the South American continent, as shown in Table 2, is

0.7976×10^{17} N, and the geometric features of these two continents allow us to ideally estimate a final horizontal force of 3.0×10^{17} N for the North American continent. We assume 45% of this force is finally transformed into the push force F_{PN}. Most of the North American plate moves away from the Mid-Atlantic Ridge and in an approximately southwest direction. We assume the push force F_{PN} to be oriented in a southwest direction, with an orientation of approximately 190° with respect to latitude. Referring to Table 2, the final horizontal force for the Australian plate is 1.8212×10^{17} N, given that 45% of this force is finally transformed into the push force F_{PA}. The Australian plate moves dominantly in the northeast direction; thus, we assume the push force F_{PA} to be finally oriented in a northeast direction. The inclination of this direction to latitude is approximately 59.43°, as listed in Table 3. Subsequently, the combined force of these two forces on the Pacific plate can be written as $F_P=(F_{PN}^2+F_{PA}^2-2F_{PN}F_{PA}\cos(\alpha-(\beta-180^o)))^{0.5}$, where $\alpha=59.43°$ and $\beta=190°$. The final horizontal force would be $F_P=1.0271\times10^{17}$ N, given that 80% of this force is used to drive the Pacific plate, 20% of this force is used to oppose the collisional force and shearing forces. Finally, we apply equation (2) to resolve the Pacific plate's speed, i.e., $u=F_{driving}\, y/\mu A$, where $F_{driving}=0.8\times F_P=0.8217\times10^{17}$ N; y is the asthenospheric thickness, y=300 km; A is the Pacific plate's area, and A=103,300,000.00 km^2. As mentioned earlier, the asthenosphere viscosity is not exactly determined and ranges from 10^{15} Pa s to 10^{20} Pa s based on various methods (e.g., laboratory experiments, glacial isostatic adjustment, and geoid modeling). This reality allows us to adopt $\mu=1.2\times10^{17}$ Pa s. The movement's orientation is determined by the final horizontal force and may be expressed as $\Delta\theta=\beta-\gamma$ and $\cos\gamma=(F_P^2+F_{PN}^2-F_{PA}^2)/(2F_PF_{PN})$. The calculated movement for this plate is further listed in Table 3.

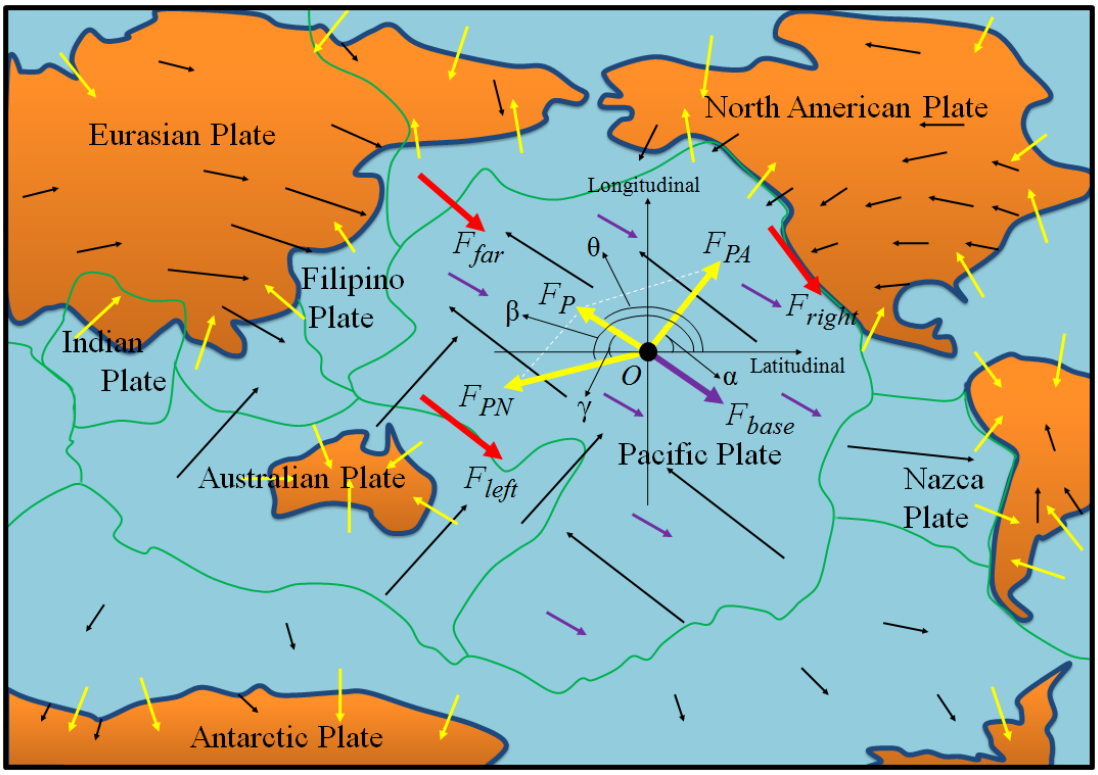

Figure 7. Modeling the dynamics of the Pacific plate. The black, yellow (thin), red, and purple (thin) arrows denote movements of plates, horizontal forces generated by oceans, resistive forces from adjacent plates, and basal friction forces, respectively. F_P, F_{PA}, and F_{PN} denote the final horizontal force exerted on the hypothetical center of geometry of the Pacific plate, the push force from the Australian plate on the hypothetical center of geometry, and the push force from the North American plate on the hypothetical center of geometry, respectively. F_{far}, F_{left}, F_{right}, and f_{base} denote the total collisional force from the part of the North American plate and the Eurasian plate , the total shearing force from the Australian plate, the total shearing force from the North American plate, and the total basal friction force exerted by the underlying asthenosphere. *O* denotes the hypothetical center of geometry of the Pacific plate. α, β, and θ are the inclination of the push force F_{PA}, the push force F_{PN}, and the final horizontal force F_P to the latitudinal direction, respectively. γ is the angle of the push force F_{PN} and the final horizontal force F_P. Note that the push force F_{PN}(F_{PA}) is approximately parallel to the North American (Australian) plate's motion. The black dot denotes the hypothetical center of geometry of the plate.

Table 3 The calculated movements for the selected five plates

Plate	Speed (u)	N Vel.	E Vel.	Inclination to latitude (Δθ), east
	mm/yr	mm/yr	mm/yr	degrees(^{o})
South America	9.11	9.00	-1.43	99.03
Africa	28.27	18.81	21.11	41.70
India	54.88	34.39	42.77	38.80
Australia	64.21	55.29	32.66	59.43
Pacific	62.71	28.77	-55.73	152.69

3.2 A torque balance solution for plate motion

The movements resolved through force balance are consistent with observation, this match provides evidence that the ocean-generated force may have capability to drive plate motion. However, if one wants to use the ocean-generated force to reach an exact solution for plate motion, more details must be considered. Conventionally, plate motion is understood as a rigid plate rotating about an axis that penetrates the Earth's center, this rotation is a consequence of the integrated effect of all torques acting on the plate (e.g., Richardson, 1992; Forsyth & Uyeda, 1975). Following this routine, we here develop a torque balance model to resolve plate motion.

As shown in Figure 8, the Earth's surface is assumed to be covered with Plate A, Plate B, Plate C, and Plate D. For Plate A, the horizontal force F_i (i=1, 2, 3, 4, and 5*)* acts on the side of the continent that is located on the top of the plate. We at first use the horizontal force to yield a component that is orthogonal to the axis of rotation of the plate, this component then yields a torque. The torques yielded by all the decomposed components are summed into a final torque, we further divide this final torque into two parts to respectively balance the torques yielded by the shearing force, collisional force, and basal force, by which an average movement is resolved for the plate. Using this movement and Euler pole location, the movement of any location of a plate may be obtained. The component yielded by the horizontal force may be expressed as $F_{i'}$= $F_i\cos\eta_i$, and $\eta_i=\gamma_i-\lambda_i$, γ_i is the inclination of the horizontal force to latitude. Both F_i and γ_i are already listed in Table 1 and 2. λ_i is the azimuth of arc P_iE with respect to latitude. This component creates a torque τ_i with respect to the axis of rotation, i.e., $\tau_i=r_i F_{i'}$, where r_i denotes lever arm distance of the component $F_{i'}$, and $r_i=R_{\text{earth}}\sin\varphi_{Pi}$, R_{earth} is the Earth's radius and R_{earth}=6,370 km, φ_{Pi} is the angle of site P_i and Eule pole.

A sum of the torques yielded by all the components reaches a final torque $\tau = \sum_{i=1}^{n} \tau_i$.

Given Plate A rotates clockwise, this rotation makes the plate undergo the shearing force $F_{shearing\text{-}f}$ from Plate B, the shearing force $F_{shearing\text{-}n}$ from Plate D, the collisional force $F_{collisional}$ from Plate C, and the basal friction force F_{basal} from the asthenosphere. These forces also create torques with respect to the axis of rotation. Here, we separate the final torque into two parts to exert: one, as an opposing torque, balances the torques caused by the collisional force and shearing forces, and the other, as a driving torque, balances the torque caused by basal friction force. As mentioned in the section 3.1.2, the movements of most of plates are intersecting with each other, these nonparallel movements would yield additional collisional and shearing forces. We here assume that all the horizontal forces yield components, by which some torques are created to balance the torques formed by these additional collisional and shearing forces. These balances of torques allow the plate to be steadily rotated around the axis of rotation under the assumption that the acceleration and inertia of plate are neglected. The balance between the driving torque and the torque caused by basal friction force may be written as

$$\tau_{driving} - \tau_{basal} = 0 \qquad (3)$$

where $\tau_{driving}$ denotes the driving torque and $\tau_{driving} = \varepsilon\tau$, ε is the ratio of the driving torque and the final torque. τ_{basal} denotes the torque yielded by the basal friction force. The torque τ_{basal} can be written as $\tau_{basal} = r_b F_{basal}$, where r_b denotes lever arm distance of basal friction force, and $F_{basal} = \mu Au/y$, μ, A, u, and y are the viscosity of the asthenosphere, the plate's area, the plate's speed, and the thickness of the asthenosphere, respectively. Therefore, $u = y\tau_{driving}/\mu A$, this speed represents an average level of the plate's movement. In practice, the largest speed of a plate occurs at the equator of the plate, while the smallest one occurs at the location whose angle distance to Euler pole is the minimum. We assume the hypothetical geometric center (i.e., location *K*) of the plate to move at the average speed, namely, $u = u_k$, and then, the speed of any location *S* within the plate may be expressed with $u_s = u_k \sin\varphi_s / \sin\varphi_k$, where φ_s (φ_k) is the angle distance of location *S* (*K*) to Euler pole (i.e., location *E*) relative to the Earth's center. The speed u_s can be further decomposed into the longitudinal speed $u_{s\text{-}lo}$ and latitudinal speed $u_{s\text{-}la}$, and $u_{s\text{-}lo} = u_s \sin(\lambda_s - 90^o)$, $u_{s\text{-}la} = u_s \cos(\lambda_s - 90^o)$, where λ_s is the azimuth of arc *SE* with respect to latitude. The

movement's azimuth is calculated through the longitudinal and latitudinal speed. All these angles and distances (i.e., η_i, γ_i, λ_i, λ_s, φ_{Pi}, φ_k, φ_s, r_i, r_b) can be obtained through the latitude and longitude of related locations.

We plot global plates into a grid of $10^o \times 20^o$, and select these nodes of grid, which are within the plate, as the sample locations of these five plates (Figure 9). Totally, 121 sites are extracted from the grid (20 for South American, 35 for African, 19 for Australian, 4 for Indian, and 43 for Pacific Plate). The hypothetical geometric center of the plate is determined by an average of the latitude and longitude of the sample locations. Euler pole location for each of these plates is referred to GSRM v.2.1 (e.g., Global Strain Rate Model) (Kreemer et al., 2014). Taking these basic ideas and referring to Figure 4, Table 1, and Table 2, the torques yielded by the horizontal forces and the movements of these sample locations are calculated through equation (3). The parameters for calculation and the resulting torques and movements for these five plates are listed in Table 4, Table 5, and Table 6. Note that the net torque of the Pacific plate is calculated through the final horizontal force F_P exhibited in Figure 7.

There are many plate motion models (i.e., GSRM, NUVEL-1, and MORVEL) that include GNSS and paleomagnetic data. For instance, GSRM v.2.1 include more than 6739 continuous GPS velocity measurements (Kreemer et al., 2014). The movements reproduced by these models may approximately represent observation. Here, the movements of these 121 sample locations are extracted from GSRM v.2.1. The calculated and extracted movements for these locations are then compared in Table 6. The calculated movements for these 121 locations are well consistent with the extracted movements in both speed and azimuth, the error between them is less than 0.8 mm/yr in speed and 0.3^o in azimuth.

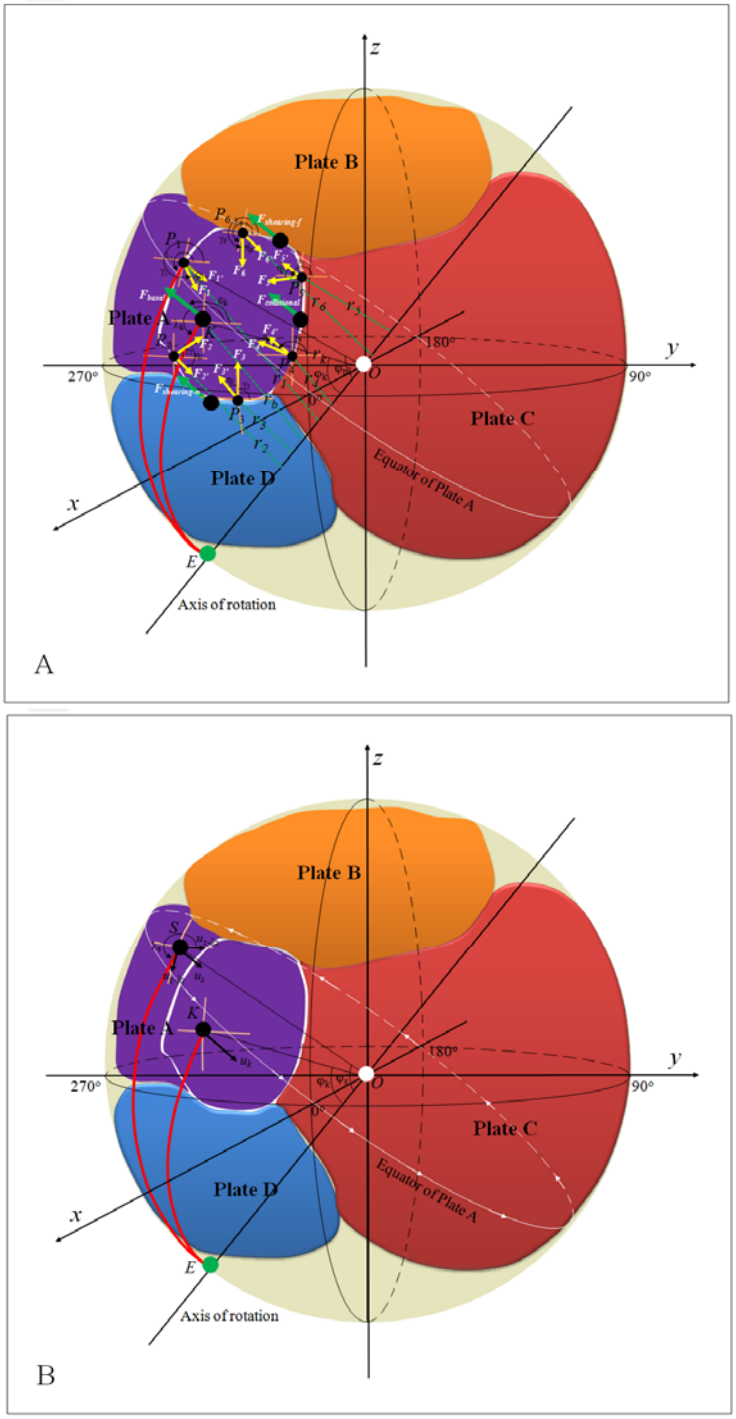

Figure 8. Modelling plate motion from torque balance. (A) Geometry of the horizontal forces and resistive forces over a spherical frame. White irregular circle within Plate A represents the scope of the continent. The pink lines beneath the locations (black dots) denote latitudinal and longitudinal direction. **(B) Decomposing the average speed of the plate into the speed of any location.** The arrows in the large white circle denote the movement's orientation of the plate.

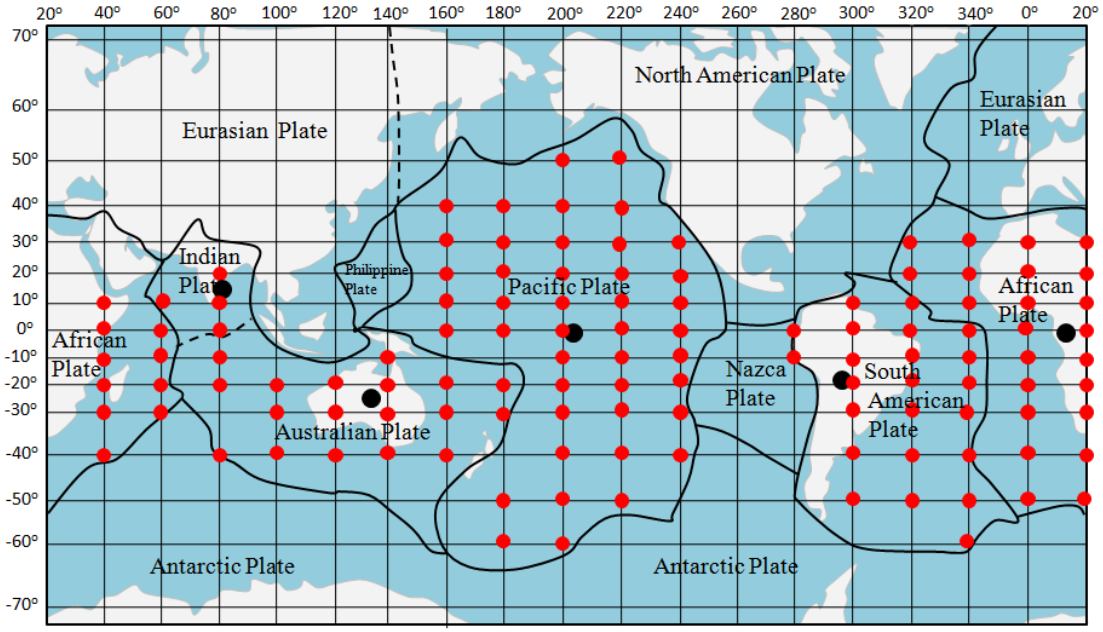

Figure 9. A global view of the sample locations of the selected five plates. Black dots within the plates represent the hypothetical geometric center of the plate. Red dots denote the sample locations.

Table 4(A). Parameters and ocean-generated torque for the selected five plates

Plate	Eule pole		No.	the azimuth of arc P_iE with respect to latitude	Angle between horizontal force and its decomposed force	Decomposed horizontal force	Angle of site P_i and Eule pole	Length of lever arm	Force direction relative to Eule pole	Torque
	E			λ_i	η_i	$F_{i'}$	φ_{Pi}	r_i		τ
	Latitude (^{o})	Longitude (^{o})	i	Degrees (°)		N (*10^{17})	Degrees (°)	m (*10^3)		N·m (*10^{23})
South America	-14.10	242.14	1	294.38	41.95	0.5474	42.97	4341.80	clockwise	+1.7679
			2	285.57	70.10	0.4844	38.80	3991.43	clockwise	+0.6580
			3	271.78	115.15	1.2425	38.74	3986.41	counterclockwise	-2.1047
			4	270.90	140.04	0.8143	42.89	4335.58	counterclockwise	-2.7059
			5	282.50	75.55	0.9821	45.41	4536.31	clockwise	+1.1116
			6	292.73	60.73	0.5650	45.77	4564.08	clockwise	+1.2610
			7	299.76	36.37	0.3731	45.77	4564.11	clockwise	+1.3713
			8	309.75	39.42	0.7500	46.27	4603.18	clockwise	+2.6669
			9	321.97	26.42	0.4902	47.93	4728.25	clockwise	+2.0758
			10	331.02	31.20	0.4355	49.71	4858.79	clockwise	+1.8102
			11	337.07	60.30	0.3916	52.05	5023.06	clockwise	+0.9746
			12	339.48	84.75	0.3391	54.79	5204.75	clockwise	+0.1615
			13	336.02	140.61	0.2650	56.65	5320.95	counterclockwise	-1.0899
			14	331.32	97.10	0.5409	55.74	5264.90	counterclockwise	-0.3521
			15	324.32	185.39	0.0907	54.05	5157.00	counterclockwise	-0.4657
			16	318.03	95.94	0.3229	53.33	5109.13	counterclockwise	-0.1707
			17	315.21	171.89	0.0360	53.01	5087.95	counterclockwise	-0.1813

18	310.51	212.51	0.5820	53.33	5109.18	counterclockwise	-2.5076
19	305.25	195.58	0.5407	53.75	5136.83	counterclockwise	-2.6752
20	301.87	152.08	0.3618	56.11	5287.51	counterclockwise	-1.6904
21	297.69	198.64	0.8890	59.24	5473.92	counterclockwise	-4.6111
22	290.35	211.98	1.2741	62.57	5653.72	counterclockwise	-6.1101
23	283.47	227.47	0.5067	65.88	5813.78	counterclockwise	-1.9914
24	279.00	191.03	0.5589	69.71	5974.58	counterclockwise	-3.2774
25	270.08	247.43	0.7688	74.14	6127.36	counterclockwise	-1.8079
26	270.44	240.32	1.0043	78.66	6245.73	counterclockwise	-3.1056
27	271.67	77.13	0.4897	81.29	6296.47	clockwise	+0.6867
28	279.12	31.76	0.5512	79.05	6254.01	clockwise	+2.9310
29	283.03	28.04	0.7618	73.55	6109.11	clockwise	+4.1074
30	286.31	57.74	0.3773	69.23	5955.88	clockwise	+1.1993
31	290.08	52.00	0.6201	66.08	5822.97	clockwise	+2.2229
32	295.13	65.76	0.6732	62.28	5638.90	clockwise	+1.5585
33	299.15	37.34	0.4212	57.83	5391.82	clockwise	+1.8057
34	300.87	32.45	0.3132	52.79	5073.46	clockwise	+1.3408
35	299.88	13.90	0.0545	48.19	4748.11	clockwise	+0.2511
						total	-4.8850

Note: the negative symbol "-" beneath latitude denotes south of the Earth's equator; the positive symbol "-" beneath torque denotes counterclockwise with respect to the axis of rotation, while the negative symbol "+" beneath torque denotes clockwise with respect to the axis of rotation.

Table 4(B). (continue) Parameters and ocean-generated torque for the selected five plates

Plate	Eule pole		No.	the azimuth of arc P_iE with respect to latitude	Angle between horizontal force and its decomposed force	Decomposed horizontal force	Angle of site P_i and Eule pole	Length of lever arm	Force direction relative to Eule pole	Torque
	E			λ_i	η_i	$F_{i'}$	φ_{Pi}	r_i		τ
	Latitude (^{o})	Longitude (^{o})	i	Degrees (°)		N (*10^{17})	Degrees (°)	m (*10^3)		N·m (*10^{23})
Africa	49.66	281.92	1	269.55	44.76	0.7391	53.31	5108.25	clockwise	+2.6809
			2	251.15	61.97	0.7113	53.27	5105.45	clockwise	+1.7068
			3	240.80	90.92	0.8337	54.21	5166.88	counterclockwise	-0.0689
			4	233.80	134.10	0.5642	56.90	5336.01	counterclockwise	-2.0952
			5	228.80	124.15	0.5824	60.14	5524.48	counterclockwise	-1.8064
			6	224.41	174.33	0.8406	65.06	5775.87	counterclockwise	-4.8313
			7	221.85	193.60	0.6214	71.00	6023.03	counterclockwise	-3.6375
			8	222.35	225.19	0.7482	75.55	6168.63	counterclockwise	-3.2528
			9	225.48	239.87	0.6672	78.69	6246.26	counterclockwise	-2.0920
			10	227.04	199.56	0.6880	82.66	6317.80	counterclockwise	-4.0959
			11	223.27	133.58	0.5862	87.19	6362.34	counterclockwise	-2.5709
			12	217.67	175.38	0.9328	91.84	6366.70	counterclockwise	-5.9193
			13	212.90	169.12	0.7416	96.78	6325.39	counterclockwise	-4.6067
			14	206.65	137.08	1.2378	100.96	6253.83	counterclockwise	-5.6687
			15	200.42	184.72	0.9154	105.96	6124.53	counterclockwise	-5.5875
			16	195.39	184.98	0.8696	111.79	5914.79	counterclockwise	-5.1241
			17	191.12	195.84	0.7817	117.32	5659.69	counterclockwise	-4.2560

18	189.16	255.63	0.2646	121.73	5417.90	counterclockwise	-0.3556
19	189.95	60.33	0.2945	123.77	5295.39	clockwise	+0.7721
20	193.44	46.53	0.8928	123.10	5336.37	clockwise	+3.2778
21	198.74	23.80	0.2994	120.59	5483.54	clockwise	+1.5020
22	203.07	82.44	0.3389	119.48	5545.32	clockwise	+0.2473
23	211.84	18.80	0.7346	115.80	5735.14	clockwise	+3.9879
24	225.80	79.53	0.8169	110.49	5967.18	clockwise	+0.8858
25	240.60	250.14	0.7904	109.00	6023.02	counterclockwise	-1.6169
26	267.67	116.97	0.9910	106.60	6104.40	counterclockwise	-2.7438
						total	-45.2690

Note: the negative symbol "-" beneath latitude denotes south of the Earth's equator; the positive symbol "-" beneath torque denotes counterclockwise with respect to the axis of rotation,while the negative symbol "+" beneath torque denotes clockwise with respect to the axis of rotation.

Table 4(C). (continue) Parameters and ocean-generated torque for the selected five plates

Plate	Eule pole		No.	the azimuth of arc P_iE with respect to latitude	Angle between horizontal force and its decomposed force	Decomposed horizontal force	Angle of site P_i and Eule pole	Length of lever arm	Force direction relative to Eule pole	Torque
	E			λ_i	η_i	$F_{i'}$	φ_{pi}	r_i		τ
	Latitude (^{o})	Longitude (^{o})	i	Degrees (°)		N (*10^{17})	Degrees (°)	m (*10^3)		N·m (*10^{23})
India	50.95	352.00	1	240.86	157.86	0.4153	63.81	5716.21	counterclockwise	-2.1989
			2	239.68	236.99	0.1907	67.01	5864.20	counterclockwise	-0.6092
			3	239.42	124.47	0.1457	68.08	5909.62	counterclockwise	-0.4872

	4	236.73	134.72	0.2378	70.34	5998.72	counterclockwise	-1.0039
	5	233.67	152.97	0.3298	73.45	6106.24	counterclockwise	-1.7937
	6	231.23	157.01	0.2343	76.31	6188.95	counterclockwise	-1.3347
	7	228.77	157.19	0.0734	79.13	6255.75	counterclockwise	-0.4234
	8	226.30	184.27	0.0789	82.55	6316.16	counterclockwise	-0.4967
	9	225.80	255.34	0.1459	84.44	6340.03	counterclockwise	-0.2341
	10	228.19	16.80	0.2734	82.40	6314.10	clockwise	+1.6528
	11	231.29	69.50	0.1528	79.61	6265.51	clockwise	+0.3352
	12	234.12	54.72	0.1421	77.86	6227.49	clockwise	+0.5112
	13	237.08	249.95	0.1702	76.82	6202.32	counterclockwise	-0.3619
	14	240.06	243.86	0.1961	77.06	6208.14	counterclockwise	-0.5363
	15	242.64	103.13	0.1027	77.01	6207.00	counterclockwise	-0.1448
	16	244.29	214.03	0.1727	77.71	6223.97	counterclockwise	-0.8909
	17	243.82	143.16	0.1204	79.79	6269.20	counterclockwise	-0.6040
	18	241.43	152.78	0.1474	82.48	6315.26	counterclockwise	-0.8277
	19	239.17	104.88	0.0818	84.48	6340.45	counterclockwise	-0.1332
							total	-9.5812

Note: the negative symbol "-" beneath latitude denotes south of the Earth's equator; the positive symbol "-" beneath torque denotes counterclockwise with respect to the axis of rotation,while the negative symbol "+" beneath torque denotes clockwise with respect to the axis of rotation.

Table 4(D). (continue) Parameters and ocean-generated torque for the selected five plates

Plate	Eule pole		No.	the azimuth of arc P_iE with respect to latitude	Angle between horizontal force and its decomposed force	Decomposed horizontal force	Angle of site P_i and Eule pole	Length of lever arm	Force direction relative to Eule pole	Torque
	E			λ_i	η_i	F_i,	φ_{pi}	r_i		τ
	Latitude (°)	Longitude (°)	i	Degrees (°)		N (*10^{17})	Degrees (°)	m (*10^3)		N·m (*10^{23})
			1	231.02	112.62	0.2797	93.09	6360.73	counterclockwise	-0.6842
			2	228.98	149.25	0.6029	95.38	6341.93	counterclockwise	-3.2860
			3	227.29	132.71	0.3669	98.11	6306.31	counterclockwise	-1.5694
			4	225.90	118.93	0.3295	99.54	6281.84	counterclockwise	-1.0010
			5	225.24	207.22	0.4023	101.31	6246.20	counterclockwise	-2.2344
			6	225.93	260.56	0.3198	102.95	6207.96	counterclockwise	-0.3255
			7	226.92	224.10	0.4143	104.45	6168.38	counterclockwise	-1.8354
			8	228.00	251.50	0.4191	106.28	6114.55	counterclockwise	-0.8129
Australia	33.31	36.38	9	229.35	227.42	0.7156	108.67	6034.90	counterclockwise	-2.9225
			10	229.59	187.65	0.6752	112.46	5886.84	counterclockwise	-3.9397
			11	228.71	186.91	0.7760	116.74	5688.93	counterclockwise	-4.3827
			12	227.99	197.70	0.4496	120.75	5474.52	counterclockwise	-2.3450
			13	227.02	150.68	0.3680	123.29	5324.98	counterclockwise	-1.7087
			14	225.87	187.90	0.3751	125.35	5195.39	counterclockwise	-1.9302
			15	226.14	72.18	0.2009	126.75	5104.14	clockwise	+0.3139
			16	227.53	49.12	0.2779	126.56	5116.84	clockwise	+0.9306
			17	229.14	78.84	0.3436	126.44	5124.84	clockwise	+0.3409

			18	231.43	79.14	0.5718	126.84	5097.66	clockwise	+0.5491
			19	233.89	64.52	0.4741	126.66	5110.19	clockwise	+1.0421
			20	235.76	45.26	0.3841	125.43	5190.70	clockwise	+1.4033
			21	237.11	13.55	0.1586	123.11	5335.95	clockwise	+0.8225
			22	238.12	13.79	0.1431	120.25	5502.51	clockwise	+0.7647
			23	238.93	7.12	0.2857	117.61	5644.39	clockwise	+1.6002
			24	240.03	45.26	0.3366	115.30	5759.04	clockwise	+1.3642
			25	241.95	30.32	0.6157	111.80	5914.57	clockwise	+3.1435
			26	242.01	104.21	0.0002	109.91	5989.37	counterclockwise	-0.0003
			27	240.10	103.78	0.0002	110.84	5953.38	counterclockwise	-0.0002
			28	239.55	8.05	0.0003	108.30	6047.90	clockwise	+0.0019
			29	240.62	84.00	0.0002	105.19	6147.50	clockwise	+0.0001
			30	241.41	16.45	0.0002	103.15	6202.99	clockwise	+0.0013
			31	240.79	60.73	0.0001	100.76	6258.03	clockwise	+0.0004
			32	239.60	96.41	0.0001	100.35	6266.34	counterclockwise	-0.0001
			33	239.10	6.86	0.0002	99.13	6289.26	clockwise	+0.0009
			34	238.21	72.97	0.0002	97.24	6319.15	clockwise	+0.0004
			35	236.11	83.27	0.5186	96.53	6328.69	clockwise	+0.3844
			36	234.32	58.35	0.4428	95.44	6341.27	clockwise	+1.4734
			37	232.82	57.84	0.5012	93.55	6357.78	clockwise	+1.6963
								total	total	-13.1440
Pacific	-63.09	109.63	*O*	331.61	178.92	1.0271	92.06	6365.87	counterclockwise	-6.5372

Note: the negative symbol "-" beneath latitude denotes south of the Earth's equator; the positive symbol "-" beneath torque denotes counterclockwise with respect to the axis of rotation,while the negative symbol "+" beneath torque denotes clockwise with respect to the axis of rotation.

Table 5 Parameters and calculated speed for the hypothetical geometric center of related plates

Plate	Ratio	Driving torque	Geometric center of the plate			Lever arm distance of basal friction force	Viscosity of asthenosphere	Thickness of asthenosphere	Speed
	ε	$\tau_{driving}$	K		φ_k	r_k	μ	y	u_k
		N·m (*10^{23})	Latitude (°)	Longitude (°)	Degrees (°)	m (*10^3)	Pa s (*10^{18})	m (*10^3)	mm/yr
South America	0.70	+3.1495	-23.50	316.00	69.86	5956.40	1.00	300	12.46
Africa	0.29	+13.1280	-4.32	14.59	95.03	6345.52	1.00	300	31.93
India	0.47	+4.5032	10.00	75.00	77.85	6227.32	1.00	300	57.49
Australia	0.94	+12.3554	-28.42	129.47	107.52	6074.50	0.60	300	68.24
Pacific	0.95	+6.2104	-0.23	204.65	92.06	6365.87	0.12	300	74.46

Note: the positive symbol "+" beneath torque denotes counterclockwise with respect to the axis of rotation. the negative symbol "-" beneath latitude denotes south of the Earth's equator.

Table 6(A). A comparison of plate motions between ocean-generated force model and GSRM v2.1

Plate	Site		Ocean-generated force model				GSRM v2.1				Error			
	Latitude (^{o})	Longitude (^{o})	Speed (V_s)	N Vel.($V_{s\text{-}la}$)	E Vel.($V_{s\text{-}lo}$)	Azimuth	Speed	N Vel.	E Vel.	Azimuth	Speed	N Vel.	E Vel.	Azimuth
			mm/yr	mm/yr	mm/yr	(cw from N)	mm/yr	mm/yr	mm/yr	(cw from N)	mm/yr	mm/yr	mm/yr	(cw from N)
South America	10	300.00	11.74	10.90	-4.37	338.14	12.12	11.25	-4.51	338.15	-0.38	-0.35	0.14	-0.02
	0	280.00	8.53	7.90	-3.23	337.74	8.81	8.16	-3.34	337.74	-0.28	-0.26	0.11	0.00
	0	300.00	11.37	10.90	-3.23	343.48	11.74	11.26	-3.34	343.48	-0.37	-0.36	0.11	0.00
	0	320.00	12.99	12.58	-3.23	345.59	13.42	13	-3.34	345.59	-0.43	-0.42	0.11	0.00
	-10	280.00	8.02	7.90	-1.42	349.81	8.29	8.16	-1.48	349.72	-0.27	-0.26	0.06	0.09
	-10	300.00	11.08	10.90	-1.99	349.63	11.44	11.25	-2.07	349.57	-0.36	-0.35	0.08	0.05
	-10	320.00	12.87	12.58	-2.71	347.83	13.29	12.99	-2.81	347.79	-0.42	-0.41	0.10	0.04
	-10	340.00	13.22	12.75	-3.49	344.69	13.65	13.17	-3.6	344.71	-0.43	-0.42	0.11	-0.02
	-20	300.00	10.92	10.90	-0.70	356.35	11.28	11.25	-0.73	356.29	-0.36	-0.35	0.03	0.06
	-20	320.00	12.76	12.58	-2.11	350.47	13.17	12.99	-2.19	350.43	-0.41	-0.41	0.08	0.04
	-20	340.00	13.26	12.75	-3.64	344.07	13.69	13.16	-3.76	344.05	-0.43	-0.41	0.12	0.01
	-30	300.00	10.91	10.90	0.62	3.28	11.26	11.25	0.62	3.15	-0.35	-0.35	0.00	0.12
	-30	320.00	12.66	12.58	-1.45	353.44	13.07	12.98	-1.5	353.41	-0.41	-0.40	0.05	0.03
	-30	340.00	13.27	12.75	-3.68	343.90	13.69	13.16	-3.8	343.89	-0.42	-0.41	0.12	0.01
	-40	320.00	12.60	12.58	-0.74	356.65	13	12.98	-0.77	356.61	-0.40	-0.40	0.03	0.04
	-40	340.00	13.25	12.75	-3.61	344.20	13.67	13.15	-3.72	344.20	-0.42	-0.40	0.11	0.00
	-50	300.00	11.35	10.90	3.17	16.20	11.69	11.23	3.24	16.09	-0.34	-0.33	-0.07	0.11
	-50	320.00	12.58	12.58	0.00	359.98	12.97	12.97	-0.02	359.91	-0.39	-0.39	0.02	0.07
	-50	340.00	13.20	12.75	-3.43	344.96	13.61	13.14	-3.54	344.92	-0.41	-0.39	0.11	0.04
	-60	340.00	13.13	12.75	-3.14	346.16	13.53	13.13	-3.24	346.14	-0.40	-0.38	0.10	0.02
India	20	80	56.35	37.03	42.47	48.92	55.87	36.69	42.13	48.95	0.48	0.34	0.34	-0.03
	10	60	54.70	34.35	42.57	51.10	54.24	34.05	42.22	51.11	0.46	0.30	0.35	-0.02

	10	80	58.08	37.03	44.75	50.40	57.58	36.70	44.37	50.40	0.50	0.33	0.38	-0.01
	0	80	58.79	37.03	45.67	50.97	58.29	36.70	45.28	50.97	0.50	0.33	0.39	-0.01
	-10	80	61.95	41.26	46.22	48.25	61.52	40.98	45.88	48.23	0.43	0.28	0.34	0.02
	-10	140	68.50	58.12	36.25	31.96	68.07	57.74	36.04	31.97	0.43	0.38	0.21	-0.02
	-20	80	66.17	41.26	51.73	51.43	65.67	40.97	51.33	51.40	0.50	0.29	0.40	0.03
	-20	100	70.62	53.57	46.01	40.66	70.13	53.21	45.68	40.65	0.49	0.36	0.33	0.01
	-20	120	71.19	59.43	39.20	33.41	70.72	59.02	38.95	33.42	0.47	0.41	0.25	-0.01
	-20	140	66.40	58.12	32.11	28.92	65.98	57.72	31.95	28.97	0.42	0.40	0.16	-0.05
	-20	160	55.99	49.80	25.60	27.21	55.66	49.46	25.53	27.30	0.33	0.34	0.07	-0.09
	-20	180	40.95	35.47	20.46	29.98	40.73	35.23	20.45	30.13	0.22	0.24	0.01	-0.16
	-30	100	71.48	53.57	47.32	41.45	70.95	53.18	46.97	41.45	0.53	0.39	0.35	0.00
Australia	-30	120	70.20	59.43	37.35	32.15	69.71	59.00	37.13	32.18	0.49	0.43	0.22	-0.03
	-30	140	64.08	58.12	26.99	24.91	63.66	57.70	26.89	24.99	0.42	0.42	0.10	-0.08
	-30	160	52.78	49.80	17.48	19.34	52.44	49.44	17.49	19.48	0.34	0.36	-0.01	-0.14
	-30	180	36.84	35.47	9.96	15.68	36.63	35.21	10.07	15.96	0.21	0.26	-0.11	-0.28
	-40	80	71.12	41.26	57.93	54.54	70.54	40.93	57.46	54.54	0.58	0.33	0.47	0.01
	-40	100	71.39	53.57	47.18	41.37	70.84	53.15	46.83	41.38	0.55	0.42	0.35	-0.01
	-40	120	68.66	59.43	34.37	30.05	68.15	58.97	34.18	30.10	0.51	0.46	0.19	-0.05
	-40	140	61.81	58.12	21.05	19.91	61.37	57.67	21.01	20.02	0.44	0.45	0.04	-0.11
	-40	160	50.57	49.80	8.82	10.04	50.21	49.41	8.92	10.23	0.36	0.39	-0.10	-0.19
	-50	160	49.80	49.80	-0.10	-0.12	49.38	49.38	0.07	0.08	0.42	0.42	-0.17	-0.20

Note: the negative symbol "-" beneath latitude denotes south of the Earth's equator.

Table 6(B). (continue) A comparison of plate motions between ocean-generated force model and GSRM v2.1

Plate	Site		Ocean-generated force model				GSRM v2.1				Error			
	Latitude (°)	Longitude (°)	Speed (V_s)	N Vel.($V_{s\text{-}la}$)	E Vel.($V_{s\text{-}lo}$)	Azimuth	Speed	N Vel.	E Vel.	Azimuth	Speed	N Vel.	E Vel.	Azimuth
			mm/yr	mm/yr	mm/yr	(cw from N)	mm/yr	mm/yr	mm/yr	(cw from N)	mm/yr	mm/yr	mm/yr	(cw from N)

	30	320	18.24	12.80	12.99	45.43	18.12	12.68	12.95	45.60	0.12	0.12	0.04	-0.17
	10	320	24.78	12.80	21.22	58.91	24.59	12.68	21.06	58.95	0.19	0.12	0.16	-0.04
	0	340	30.12	17.61	24.43	54.21	29.86	17.46	24.22	54.21	0.26	0.15	0.21	0.00
	30	340	23.58	17.61	15.67	41.67	23.39	17.44	15.59	41.79	0.19	0.17	0.08	-0.13
	30	0	27.82	20.30	19.02	43.13	27.58	20.11	18.88	43.19	0.24	0.19	0.14	-0.07
	30	20	30.55	20.54	22.62	47.75	30.28	20.35	22.43	47.78	0.27	0.19	0.19	-0.03
	20	320	21.58	12.80	17.37	53.62	21.42	12.68	17.27	53.71	0.16	0.12	0.10	-0.09
	20	340	26.06	17.61	19.21	47.48	25.85	17.45	19.07	47.54	0.21	0.16	0.14	-0.06
	20	0	29.56	20.30	21.49	46.63	29.32	20.12	21.33	46.67	0.24	0.18	0.16	-0.04
	20	20	31.56	20.54	23.96	49.39	31.28	20.36	23.75	49.39	0.28	0.18	0.21	-0.01
	10	340	28.30	17.61	22.16	51.52	28.07	17.46	21.98	51.54	0.23	0.15	0.18	-0.02
	10	0	30.92	20.30	23.32	48.95	30.65	20.12	23.12	48.97	0.27	0.18	0.20	-0.01
	10	20	32.02	20.54	24.57	50.10	31.75	20.36	24.35	50.10	0.27	0.18	0.22	0.00
Africa	0	0	31.77	20.30	24.43	50.28	31.49	20.12	24.22	50.28	0.28	0.18	0.21	-0.01
	0	20	31.92	20.54	24.43	49.94	31.64	20.36	24.22	49.95	0.28	0.18	0.21	-0.01
	-10	0	32.05	20.30	24.80	50.70	31.77	20.12	24.59	50.71	0.28	0.18	0.21	-0.01
	-10	20	31.25	20.54	23.55	48.91	30.99	20.36	23.36	48.93	0.26	0.18	0.19	-0.02
	-20	0	31.76	20.30	24.42	50.27	31.48	20.12	24.21	50.27	0.28	0.18	0.21	-0.01
	-20	20	30.07	20.54	21.96	46.91	29.82	20.36	21.79	46.94	0.25	0.18	0.17	-0.03
	-30	0	30.90	20.30	23.30	48.94	30.63	20.11	23.11	48.97	0.27	0.19	0.19	-0.04
	-30	20	28.46	20.54	19.70	43.80	28.22	20.35	19.56	43.87	0.24	0.19	0.14	-0.07
	-40	0	29.55	20.30	21.47	46.60	29.28	20.10	21.30	46.66	0.27	0.20	0.17	-0.06
	-40	20	26.56	20.54	16.84	39.34	26.33	20.34	16.73	39.44	0.23	0.20	0.11	-0.09
	-50	0	27.80	20.30	18.99	43.08	27.54	20.09	18.84	43.16	0.26	0.21	0.15	-0.08
	-50	20	24.57	20.54	13.47	33.25	24.34	20.32	13.40	33.40	0.23	0.22	0.07	-0.15
	10	40	31.60	18.31	25.76	54.60	31.32	18.15	25.53	54.59	0.28	0.16	0.23	0.01
	0	40	30.53	18.31	24.43	53.16	30.27	18.15	24.22	53.15	0.26	0.16	0.21	0.00

0	60	28.09	13.86	24.43	60.43	27.85	13.74	24.22	60.43	0.24	0.12	0.21	0.00
-10	40	28.90	18.31	22.36	50.70	28.66	18.15	22.19	50.72	0.24	0.16	0.17	-0.02
-10	60	25.48	13.86	21.38	57.04	25.28	13.74	21.22	57.08	0.20	0.12	0.16	-0.04
-20	40	26.83	18.31	19.62	46.98	26.62	18.14	19.48	47.04	0.21	0.17	0.14	-0.06
-20	60	22.46	13.86	17.68	51.90	22.30	13.74	17.57	51.97	0.16	0.12	0.11	-0.08
-30	40	24.49	18.31	16.28	41.64	24.30	18.13	16.18	41.75	0.19	0.18	0.10	-0.11
-30	60	19.31	13.86	13.44	44.11	19.18	13.73	13.39	44.28	0.13	0.13	0.05	-0.17
-40	40	22.13	18.31	12.44	34.19	21.95	18.12	12.39	34.36	0.18	0.19	0.05	-0.17

Note: the negative symbol "-" beneath latitude denotes south of the Earth's equator.

Table 6(C). (continue) A comparison of plate motions between ocean-generated force model and GSRM v2.1

Plate	Location		Ocean-generated force model				GSRM v2.1				Error			
	Latitude (^{o})	Longitude (^{o})	Speed (V_s)	N Vel.($V_{s\text{-}la}$)	E Vel.($V_{s\text{-}lo}$)	Azimuth	Speed	N Vel.	E Vel.	Azimuth	Speed	N Vel.	E Vel.	Azimuth
			mm/yr	mm/yr	mm/yr	(cw from N)	mm/yr	mm/yr	mm/yr	(cw from N)	mm/yr	mm/yr	mm/yr	(cw from N)
Pacific	50	200	54.28	33.72	-42.54	308.40	53.79	33.33	-42.22	308.29	0.49	0.39	-0.32	0.11
	50	220	46.22	31.61	-33.71	313.16	45.83	31.25	-33.52	312.99	0.39	0.36	-0.19	0.16
	40	160	69.74	25.97	-64.72	291.86	69.06	25.68	-64.1	291.83	0.68	0.29	-0.62	0.03
	40	180	66.28	31.76	-58.18	298.63	65.66	31.41	-57.66	298.58	0.62	0.35	-0.52	0.05
	40	200	60.93	33.72	-50.75	303.60	60.39	33.35	-50.35	303.52	0.54	0.37	-0.40	0.08
	40	220	53.65	31.61	-43.35	306.10	53.21	31.26	-43.05	305.98	0.44	0.35	-0.30	0.12
	30	160	73.06	25.97	-68.29	290.82	72.35	25.7	-67.63	290.81	0.71	0.27	-0.66	0.01
	30	180	70.73	31.76	-63.20	296.68	70.06	31.43	-62.62	296.65	0.67	0.33	-0.58	0.03
	30	200	66.60	33.72	-57.43	300.42	65.99	33.37	-56.93	300.38	0.61	0.35	-0.50	0.04
	30	220	60.57	31.61	-51.67	301.46	60.05	31.28	-51.26	301.39	0.52	0.33	-0.41	0.07
	30	240	53.23	25.69	-46.62	298.86	52.81	25.42	-46.29	298.77	0.42	0.27	-0.33	0.09
	20	160	74.46	25.97	-69.79	290.41	73.73	25.71	-69.1	290.41	0.73	0.26	-0.69	0.00
	20	180	73.52	31.76	-66.31	295.59	72.82	31.44	-65.68	295.58	0.70	0.32	-0.63	0.01

20	200	70.89	33.72	-62.36	298.40	70.23	33.38	-61.79	298.38	0.66	0.34	-0.57	0.02
20	220	66.42	31.61	-58.42	298.42	65.83	31.3	-57.91	298.39	0.59	0.31	-0.51	0.03
20	240	60.67	25.69	-54.96	295.05	60.15	25.43	-54.51	295.01	0.52	0.26	-0.45	0.04
10	160	73.88	25.97	-69.16	290.58	73.16	25.72	-68.49	290.58	0.72	0.25	-0.67	0.00
10	180	74.50	31.76	-67.40	295.23	73.79	31.45	-66.75	295.23	0.71	0.31	-0.65	0.00
10	200	73.57	33.72	-65.39	297.28	72.88	33.39	-64.78	297.27	0.69	0.33	-0.61	0.01
10	220	70.84	31.61	-63.39	296.50	70.18	31.3	-62.81	296.49	0.66	0.31	-0.58	0.02
10	240	66.78	25.69	-61.64	292.63	66.17	25.44	-61.08	292.61	0.61	0.25	-0.56	0.02
0	160	71.33	25.97	-66.44	291.35	70.66	25.72	-65.81	291.35	0.67	0.25	-0.63	0.00
0	180	73.64	31.76	-66.44	295.55	72.94	31.45	-65.81	295.54	0.70	0.31	-0.63	0.01
0	200	74.51	33.72	-66.44	296.91	73.8	33.39	-65.81	296.90	0.71	0.33	-0.63	0.01
0	220	73.57	31.61	-66.44	295.45	72.88	31.31	-65.81	295.44	0.69	0.30	-0.63	0.00
0	240	71.23	25.69	-66.44	291.14	70.56	25.44	-65.81	291.13	0.67	0.25	-0.63	0.01
-10	200	73.64	33.72	-65.47	297.25	72.94	33.39	-64.85	297.24	0.70	0.33	-0.62	0.01
-10	220	74.51	31.61	-67.47	295.11	73.79	31.3	-66.82	295.10	0.72	0.31	-0.65	0.01
-10	240	73.83	25.69	-69.22	290.36	73.12	25.44	-68.55	290.36	0.71	0.25	-0.67	0.00
-20	200	71.02	33.72	-62.51	298.35	70.36	33.38	-61.94	298.32	0.66	0.34	-0.57	0.02
-20	220	73.58	31.61	-66.45	295.44	72.88	31.3	-65.81	295.44	0.70	0.31	-0.64	0.01
-20	240	74.47	25.69	-69.90	290.18	73.74	25.43	-69.22	290.17	0.73	0.26	-0.68	0.01
-30	200	66.78	33.72	-57.65	300.33	66.17	33.37	-57.15	300.28	0.61	0.35	-0.50	0.04
-30	220	70.85	31.61	-63.41	296.50	70.17	31.28	-62.82	296.47	0.68	0.33	-0.59	0.03
-30	240	73.12	25.69	-68.46	290.57	72.4	25.42	-67.79	290.56	0.72	0.27	-0.67	0.02
-40	200	61.17	33.72	-51.03	303.45	60.62	33.35	-50.62	303.38	0.55	0.37	-0.41	0.08
-40	220	66.44	31.61	-58.44	298.41	65.81	31.26	-57.91	298.36	0.63	0.35	-0.53	0.05
-40	240	69.83	25.69	-64.93	291.59	69.15	25.41	-64.31	291.56	0.68	0.28	-0.62	0.03
-50	180	46.55	31.76	-34.03	313.03	46.15	31.39	-33.83	312.86	0.40	0.37	-0.20	0.17

-50	200	54.54	33.72	-42.87	308.19	54.05	33.33	-42.55	308.07	0.49	0.39	-0.32	0.11
-50	220	60.60	31.61	-51.70	301.45	60.02	31.25	-51.25	301.37	0.58	0.36	-0.45	0.07
-60	180	39.45	31.76	-23.41	323.61	39.09	31.37	-23.31	323.39	0.36	0.39	-0.10	0.22
-60	200	47.47	33.72	-33.41	315.27	47.01	33.31	-33.17	315.12	0.46	0.41	-0.24	0.15

Note: the negative symbol "-" beneath latitude denotes south of the Earth's equator.

3. 3 Resultant stress

As mentioned in section 2, the observed stresses are mainly compressional and concentrated on the uppermost part of the lithosphere (Zoback, 1992; Zoback et al., 1989; Zoback & Magee, 1991). Our modeling of the vertical distribution of horizontal stress revealed that the stress caused by slab pull cannot be in accordance with the observed stress. This failure requires other force to be responsible for the observed stresses. Ocean-generated force may be this force. Ocean is loaded on the top of the lithosphere, the region along which the ocean-generated force is exerted is topographically higher, it is easy for this force to form a stress field associated with the uppermost brittle part of the lithosphere.

A simple model is developed to demonstrate the stress produced by the ocean-generated force. The model consists the Earth's crust that is loaded with ocean. The crust is straight, and its length and height are 7,500 km and 50 km, respectively. The ocean depth varies from 5.0 km on the left to 4.0 km on the right. The crust is composed of rocks and is assumed to be homogeneous and isotropic. We employ finite element analysis software (i.e., Abaqus) to resolve the resultant stress. The model's bottom is given a remote boundary condition, and there are no edge boundary condition for the left and right ends of the model. A 50 km depth of crust represents the lithosphere's upper part, which is mostly elastic, therefore the ductile nature may be neglected. The inputs are the crust's pressure caused by its weight and the ocean's hydrostatic pressure. The outputs include two sets of data: one is the stress produced by the crust's pressure alone, and the other is the stress produced by a combination of the crust's pressure and the ocean's pressure. The two-dimensional frame allows us to obtain a horizontal stress S11 and a vertical stress S22. To realize a quantitative solution, we select the stress at 10 sites of the model to compare. The model and the resultant stress are shown in Figure 10, and the simulated stress of the selected ten sites and some of the parameters utilized in the calculation are further listed in Table 7. It can be found that ocean water has a significant impact on the crust's stress, the stress produced by ocean water is mainly compressional and penetrates the entire thickness of the crust. Along the horizontal direction, the maximal stress S11, approximately 5.4 ~ 12.5 MPa, dominates the uppermost part of the crust that is within a depth of ~ 20 km. The mean stress of this depth is 2.7 ~ 8.04 Mpa; Along the

vertical direction, the maximal stress S22, approximately 13.1 ~ 15.8 Mpa, dominates more than 40 km depth. The mean stress of this depth is 3.84 ~ 8.58 Mpa. The observed stresses (i.e., deviatoric stresses) in the upper parts of the intraplate regions have general magnitudes of 20~30 MPa (Forsyth & Uyeda, 1975; Bott and Kusznir, 1984; Zoback & Magee, 1991; Fialko et al., 2005). The deviatoric stresses in the continents are usually with the amplitude of 10 to 100 MPa (Turcotte and Schubert, 2002). In this point, the stress caused by ocean water is in accordance with the observed stress in vertical distribution, style, and amplitude. It is important to note that this model does not include collisional force and basal friction; in practice, the Earth's crust is curved, the crustal rocks are not homogeneous and isotropic, and the crust's thickness and density also vary spatially; in addition, as seen in Figure 11, the directions of ocean-generated force are various. We expect, the stresses caused by a combination of ocean-generated force and all of these factors may realize a better match with the observed stresses in the WSM.

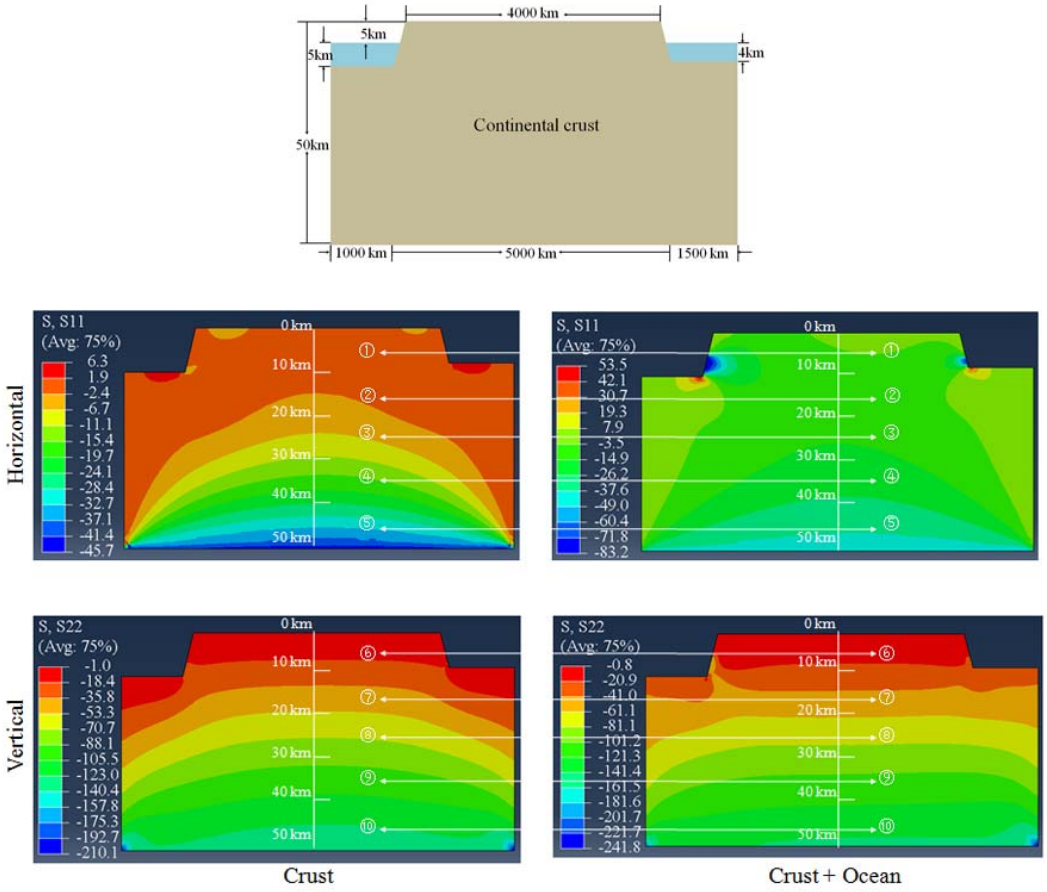

Figure 10. Modeling the stress produced by crust and ocean. Top, geometry of the model; bottom, the stress modeled by Abaqus, where the unit of stress is MPa. The negative symbol "-" denotes compressional. The numbers in the circles denote the ten selected sites in the crust.

Subsequently, a detailed investigation of the observed stress data revealed that S_{Hmax} orientations are often rotated into a plane approximately parallel to the continental slope's trend (Zoback, 1992; Zoback et al., 1989). This rotation was presently explained as a result of the superposition of stresses owing to flexure from sediment loading on the continental shelf (Dart and Zoback, 1987). Continental shelf is a part of the continent, its width is generally tens of kilometers. Sediment loading expresses mainly a weight that is added to previous topography, the stress caused by this additional weight is rather limited and very difficult to horizontally dominate the observed stresses whose orientations are subparallel and to across the plate's size of thousands of kilometers length. Instead, ocean-generated force is exerted on the slope of continent, it is natural for this force to form a stress field that follows the continental slope.

Table 7 Parameters and stresses of the selected ten sites

Water's density	Rock's density	Gravitational acceleration	Elastic modulus	Poisson ratio	Stress				
					MPa				
kg/m^3	kg/m^3	m/s^2	Mpa		Direction	Site	Crust	Crust + Ocean	Difference
1,000	2,690	9.8	100,000	0.3	Horizontal (S11)	1	1.9 ~ -2.4	-3.5~ -14.9	-5.4 ~ -12.5
						2	1.9 ~ -2.4	-3.5~ -14.9	-5.4 ~ -12.5
						3	-2.4 ~ -6.7	-3.5~ -14.9	-1.1 ~ -8.2
						4	-11.1 ~ -19.7	-14.9 ~ -26.2	-3.8~ -6.5
						5	-28.4 ~ -37.1	-26.2 ~ -37.6	+2.2 ~ -0.5
					Vertical (S22)	6	-1.0 ~ -35.8	-0.8 ~ -41.0	+0.2 ~ -5.2
						7	-35.8 ~ -53.3	-41.0~ -61.1	-5.2 ~ -7.8
						8	-53.3 ~ -88.1	-61.1 ~ -101.2	-7.8 ~ -13.1
						9	-88.1 ~ -105.5	-101.2 ~ -121.3	-13.1 ~ -15.8
						10	-128.0 ~ -140.4	-121.3~ -141.4	+6.7 ~ -1.0

Note: The negative symbol "-" denotes compressional, and the positive symbol "+" denotes extensional.

4 Discussion

All continents are being surrounded by oceans, the ocean-generated forces are extensively exerted on the sides of the continents that are fixed on the top of the lithospheric plates, and all plates connect to each other, as a consequence, the interactions of all the plates may result in plate motions across the globe (Figure 11). Under the effect of ocean-generated force, a moving continental plate would ride on an oceanic plate when these two plates meet, the front part of the oceanic plate is forced to subduct, forming sinking slab; Also, a moving plate would move away from another plate, a gap forms between them. The gap, if deep enough, allows magma to erupt, forming a MOR. As ocean-generated force is exerted on the continent's wall (represented with the coastline), the oceanic crust is extensively connected to the continental crust, this linkage allows ocean-generated force to be laterally transferred to the oceanic crust, and then, the continental crust drags the oceanic crust to lead the plate's boundary shape to follow the coastline's shape.

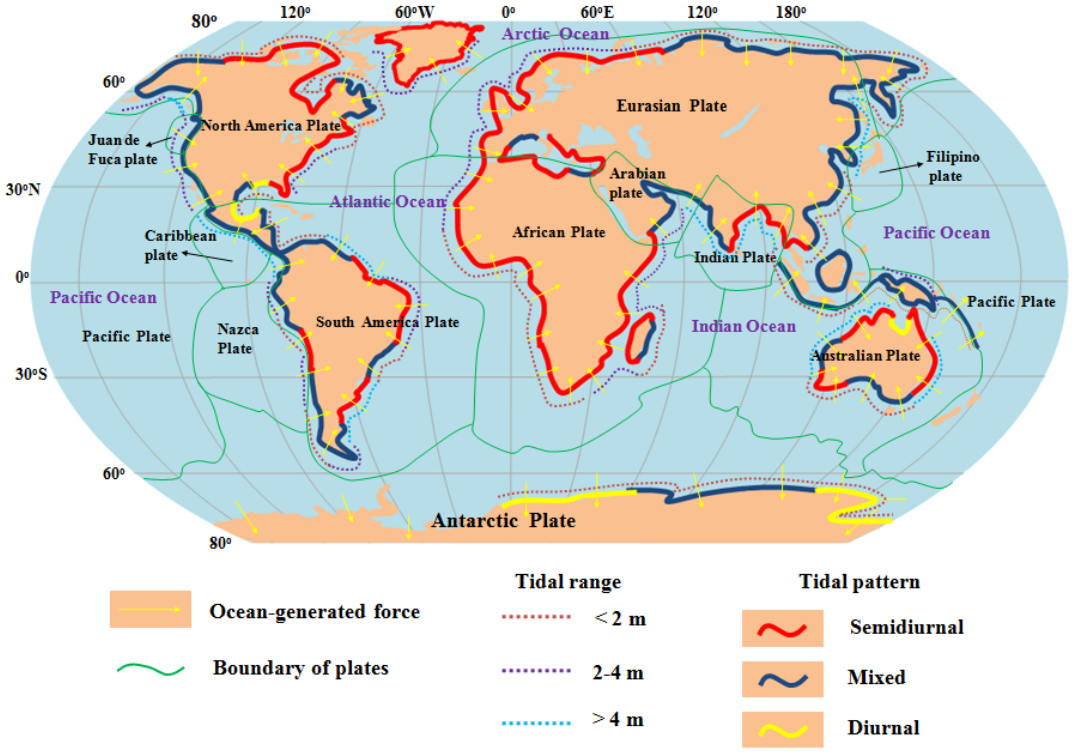

Figure 11. Global view of the distribution of plate tectonics and ocean-generated forces. The supporting tidal data are mainly from GLOSS database (e.g., the Global Sea Level Observing System) (Caldwell et al. 2015).

Although we have demonstrated in section 3 that ocean-generated force may have capability to drive plate motion, many people still oppose this force as plate driving force. Their reasons for rejecting this force include: 1) ocean constitutes just another deviation from a truly radial density distribution of the Earth. Any "lateral" density heterogeneity creates stresses that in turn lead to deformation, their extent is controlled by the rheological properties of the involved materials; 2) plate motion determines the shape of ocean basin, as a result, ocean water cannot drive plate to move; 3) ocean loading on the top of the lithosphere doesn't allow ocean-generated force to drive the lithospheric plates to move along the asthenosphere. For instance, the water hold in a container standing on the ground cannot drive the container to move along the ground; 4) ocean-generated force is too small to drive plate motion. These issues need to be clarified here. First of all, the view that any "lateral" density heterogeneity would lead denser materials (i.e., rocks) to move towards lighter materials (i.e., air or water) is rather idealized. The Himalayas is denser than the surrounding air and water, but it does not stop moving by its density to reduce its height, instead, it increasingly rises. This counterexample provides insight that a disturbed system is unnecessary to follow the trend of "lateral" density heterogeneity. Clearly, for a system consisting of ocean water and the lithosphere it is permanently disturbed by tide, consequently, the lithospheric rocks are impossible to follow the principle of the "lateral" density heterogeneity to move towards ocean water. Indeed, plate motion may change the shape of ocean basin, but ocean water is not motionless, it may provide feedback by a dissipation of energy on plate, as a result, plate motion is affected. Ocean loading on the lithosphere is different from water loading in a container. Because the lithosphere has already been fractured into individual plates, and these plates are attached to the underlying viscous asthenosphere, this reality allows ocean-generated force to interact with the basal friction exerted by the asthenosphere on the plate. In contrast, the container is perfect, the force produced by water pressure is balanced out by the container itself and cannot interact with the basal friction exerted by the ground on the container. In physics, the interaction of a driving force and a resistive force is a precondition that an object moves.

Figure 12 outlines how ocean-generated force apparently drives plate motion. Three plates are totally designed in the model, along the vertical direction the weight of each plate is balanced out by the supporting from the asthenosphere, thus, we just need to discuss the forces along the horizontal direction. For Plate A, as the oceanic ridge

represents a boundary between the two separating plates, the ridge's crest is rift from where magma erupts, this weakness allows the ocean-generated forces F_{AR} and F_{AL}, the basal friction f_A, and the collisional force F_{BA} to interact with each other. Once these forces are equal in magnitude or close to each other, a force balance between these forces may be formed; For Plate B, it is assumed that Plate A rotates counterclockwise and Plate C rotates clockwise, these two plates give Plate B the collisional forces F_{AB} and F_{CB}, respectively, these two forces may also interact with the basal friction f_B; For Plate C, the ocean-generated forces F_{CL} and F_{CR}, the basal friction f_C, and the collisional force F_{BC} may also interact with each other. Subsequently, we discuss whether the balances between these forces can be formed or not. The lithospheric plates are moving over the Earth's surface, and all plates are connected to each other, this complexity means that the magnitude of the resistive force is not easily to be known. We here provide a method to estimate the resistive force. Since all plates are attached to the underlying viscous asthenosphere, plate motion must obey the principle of fluid mechanics. The lithosphere's thickness relative to its length (i.e., area) allows the lithosphere to be treated as a "thin" shell, we assume that the whole lithosphere is steadily moving along the viscous asthenosphere, the total basal friction force exerted by the asthenosphere along the lithosphere's base can be written as f_{basal} =μAu/y, where μ, A, u, and y are the viscosity of the asthenosphere, the lithosphere's area, the lithosphere's speed, and the thickness of the asthenosphere, respectively. Given $\mu=10^{18}$ Pa s, A=510,000,000 km^2, u=3 cm/yr, and y=300 km, then, f_{basal} =μAu/y=1.62×10^{18} N. As mentioned earlier, many numerical models yield a higher viscosity of $10^{17} \sim 10^{20}$ Pa s for the asthenosphere, while laboratory experiments yield a lower viscosity down to 10^{15} Pa s for the asthenosphere, we here adopt $\mu=10^{18}$ Pa s is appropriate. After that, the total basal friction force is allocated to individual plates based on a ratio of a plate's area and the lithosphere's area. South American, North American, African, Indian, Australian, Pacific, Eurasian, and Antarctic plates have the area of 43,600,000, 76,000,000, 61,300,000, 11,900,000, 47,000,000, 103,300,000, 67,800,000, and 60,900,000 km^2, respectively, the area ratio allows these plates to obtain a basal friction force of 1.38×10^{17} N, 2.41×10^{17} N, 1.94×10^{17} N, 3.77×10^{17} N, 1.49×10^{17} N, 3.27×10^{17} N, 2.15×10^{17} N, and 1.93×10^{17} N, respectively. Theoretically speaking, if the driving force that a plate receives is equal to this allocated basal friction force, the force balance can be formed. Table 2 shows that the ocean-generated force for South

American, African, Indian, and Australian plates are 0.7976×10^{17} N, 7.8501×10^{17} N, 1.5156×10^{17} N, and 1.8212×10^{17} N, respectively. An equality in magnitude between the ocean-generated force and the allocated basal friction force allows to form force balances for these plates. Notwithstanding, plates are moving along different directions, a plate would also receive collisional and shearing forces from its adjacent plates, therefore, to build a force balance, all related resistive forces must be included. As these adjacent plates are also attached to the underling viscous asthenosphere, the collisional force and shearing forces that these adjacent plates provide essentially arise from the basal friction exerted by the asthenosphere on them. As seen above, each of these plates is allocated a basal friction force of $\sim10^{17}$ N. Based on the calculated ocean-generated forces in Table 2, we expect that ocean-generated forces for the continental plates would have an amplitude of $\sim10^{17}$ N. And then, we conclude each of these plates may have its own force balance, by which the motion can be steadily maintained.

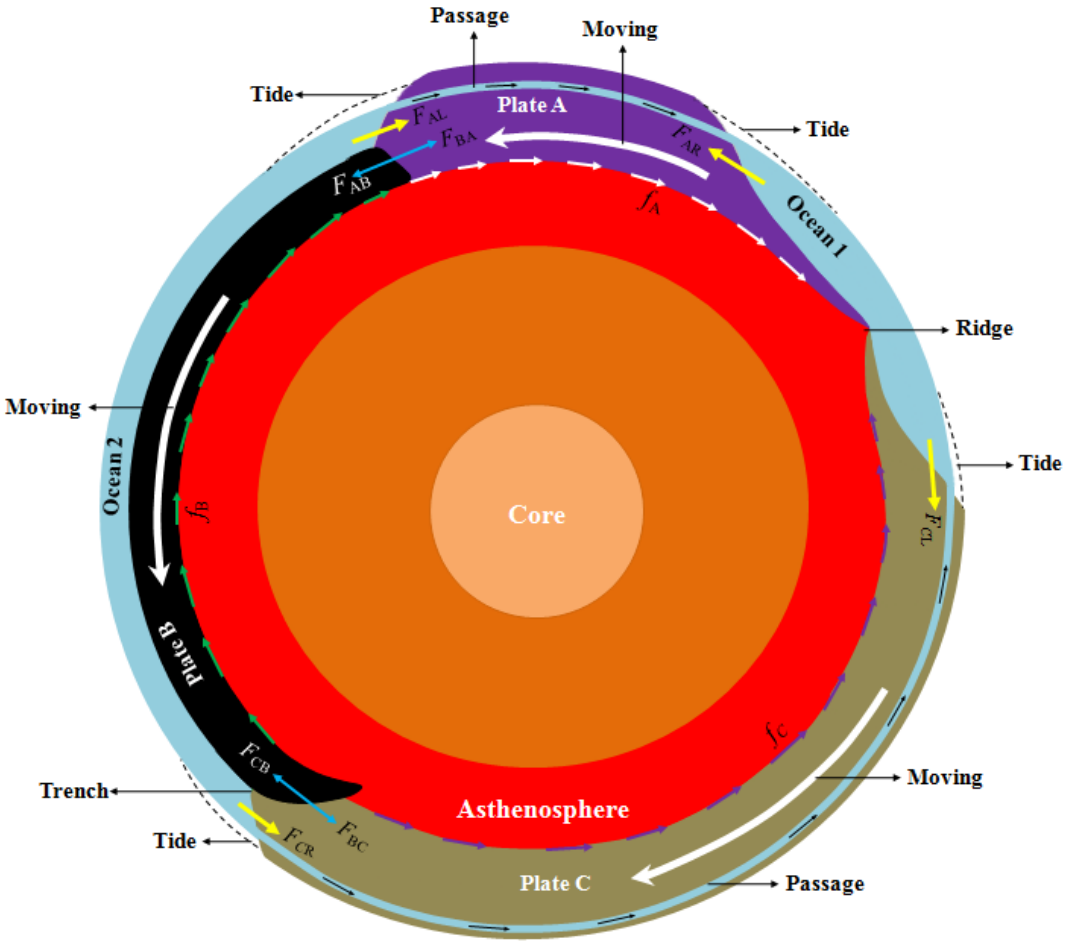

Figure 12. Modeling the dynamics of the lithospheric plates. Black arrows in the passages denote water compensation from one ocean to another. Note that the ocean depth, tide, plate size, mantle, plume, and core are highly exaggerated.

So far, we have came to a point that ocean-generated force is able to satisfy the kinematics and geometry of plate motion. Now, let's discuss how plate motion can be mechanically satisfied. As shown in Figure 12, it is assumed that the Ocean 1 depth is greater than the Ocean 2 depth. If we use a part of Ocean 2 that connects to Plate A, which is equal in length to Ocean 1, to compare, the depth difference between this part of Ocean 2 and Ocean 1 produces a net gravitational potential energy relative to the asthenosphere reference level. As Plate A and Plate B are moving away from each other, this separation would require the Ocean 1 depth to decrease as the basin elongates horizontally, and require the Ocean 2 depth to increase as the basin shortens horizontally. Consequently, the net gravitational potential energy reduces. Therefore, if there were no external energy input to compensate, the net gravitational potential energy would eventually disappear terminating plate motion. Tides may be the one to supply this energy. Tides represent the regular alternations of high and low water on the Earth, when high water falls, the gravitational potential energy converts into the kinetic energy, ocean water obtains movement. As all oceans are physically connected, part of the water in Ocean 2 may travel via passages to compensate the decreasing ocean depth in Ocean 1, by which the net gravitational potential energy is sustained. Given the basal friction force f_{basal} = 1.62×10^{18} N and the movement distance u=3 cm/yr for the lithosphere, this movement distance requires an energy Q_1= $f_{basal}\times u=4.86\times10^{16}$ J/yr to satisfy. This energy also represents the net gravitational potential energy. Ocean water is often raised twice per day due to tide and the resultant height is given h=0.3 m. Given gravitational acceleration g=9.8 m/s, the volume v=1.35×10^{9} km^3 and density ρ=1000 kg/ m^3 for ocean water, consequently, the gravitational potential energy obtained by ocean water due to the tide's raising during a year would be Q_2=2*365*ρvgh=2.9×10^{21} J/yr. The transformation from gravitational potential energy to kinetic energy within ocean water and the energy transition between oceans must be complicated, we believe that a little part of this tidal energy is enough for supplying the net gravitational potential energy. In fact, the impact of tidal energy on plate motion is long discussed. Wegener (1924) presented that tides cause a slight progressive displacement of the crust. Rochester (1973)

showed that the total energy released due to tidal friction exceeds $5*10^{19}$ ergs/s. These authors (e.g., Miller, 1966; Munk, 1968) concluded that the dissipation in both shallow seas and solid Earth is approximately $2*10^{19}$ ergs/s, and this amount of energy exceeds the lower bound set by seismic energy release by 2 orders of magnitude (Gutenberg, 1956) and might be available for driving plate motion. These authors (e.g., Riguzzi et al., 2010; Egbert and Ray, 2000) reevaluated the energy budget and found that the total energy released by tidal friction may reach up to $1.2*10^{20}$J/yr, and about $0.8*10^{20}$J/yr is dissipated in the oceans, shallow seas, and mantle, and the remaining energy is enough for maintaining the lithosphere's rotation, estimated at approximately $1.27*10^{19}$J/yr. Compared to these researches, this work provides another understanding: the tidal energy obtained by ocean water may feed plate motion.

The dispersal and aggregation of plates also reflect that the ocean basin had been periodically adjusted, and this change of ocean basin is often called the Wilson Cycle (Wilson, 1963). Figure 13 outlines how such a cycle may be realized. It is assumed that the left end of the model is connected to its right end, and that the Ocean 1 depth is greater than Ocean 2 depth. This ocean depth difference allows to yield ocean-generated force for the continental plate. The ocean-generated force, the collisional force between the plates, and the basal friction force exerted by the asthenosphere, and combine to form force balances. At the time of t_1 and t_2, Plate A and Plate B are moving towards each other, Plate C is pushed by Plate B to move, and Plate A overrides the front end of Plate C, Ocean 2 basin is shortening, while Ocean 1 basin is elongating; At the time of t_3, Plate A and Plate B meet together, forming an aggregation. Plate C entirely sinks and becomes disappeared, the Ocean 2 basin closes, and the force balances terminate. As the forming oceanic crusts cannot be spread away from the ridge, they gradually accumulate and finally close magma eruption, the ridge tends to die. After that, a large asteroid collides the aggregated plate violently, forming extensive fractures on the plate, one of the fractures penetrates down to the lower part of the lithospheric plate; At the time of t_4, the big fracture induces water to enter, forming a large body of water that is deeper than Ocean 1, the deeper water body yields greater ocean-generated force. The big fracture also reflects a mass loss of the upper part of the lithosphere, the isostasy would require the upper mantle to melt, the molten material rises, the aggregated plate is apparently divided into Plate D and Plate E. Under the effect of the ocean-generated force, the two plates tend to move

away from each other; At the time of t_5, a combination of the ocean-generated force and the rising molten material finally breaks the thickness of the plate, the new force balances are built, by which Plate D and Plate E move away from each other. A new oceanic ridge forms, and the increasingly separation between the two plates results in Ocean 3 basin. As the left end of the model is connected to its right end, the increasingly separation would also require the left part of Plate D to compress the right part of Plate E, together with the basal friction exerted by the asthenosphere on the plate, the left part of Plate D is eventually detached from the plate, forming subduction. Asteroid impacts are frequent events in the solar system, it is widely believed that the initiation of plate motion relates to large asteroid impact (Alvarez, et al., 1980; Rampino and Stothers, 1984; Prinn and Fegley, 1987; Marzoli, et al., 1999; Hames, et al., 2000; Condie, 2001; Wan, 2018), but the detail of this coupling remains elusive. Our demonstration here provides first insight on this issue: asteroid impact initiates plate motion, ocean water yields force to maintain plate motion, and tide provides energy for plate motion.

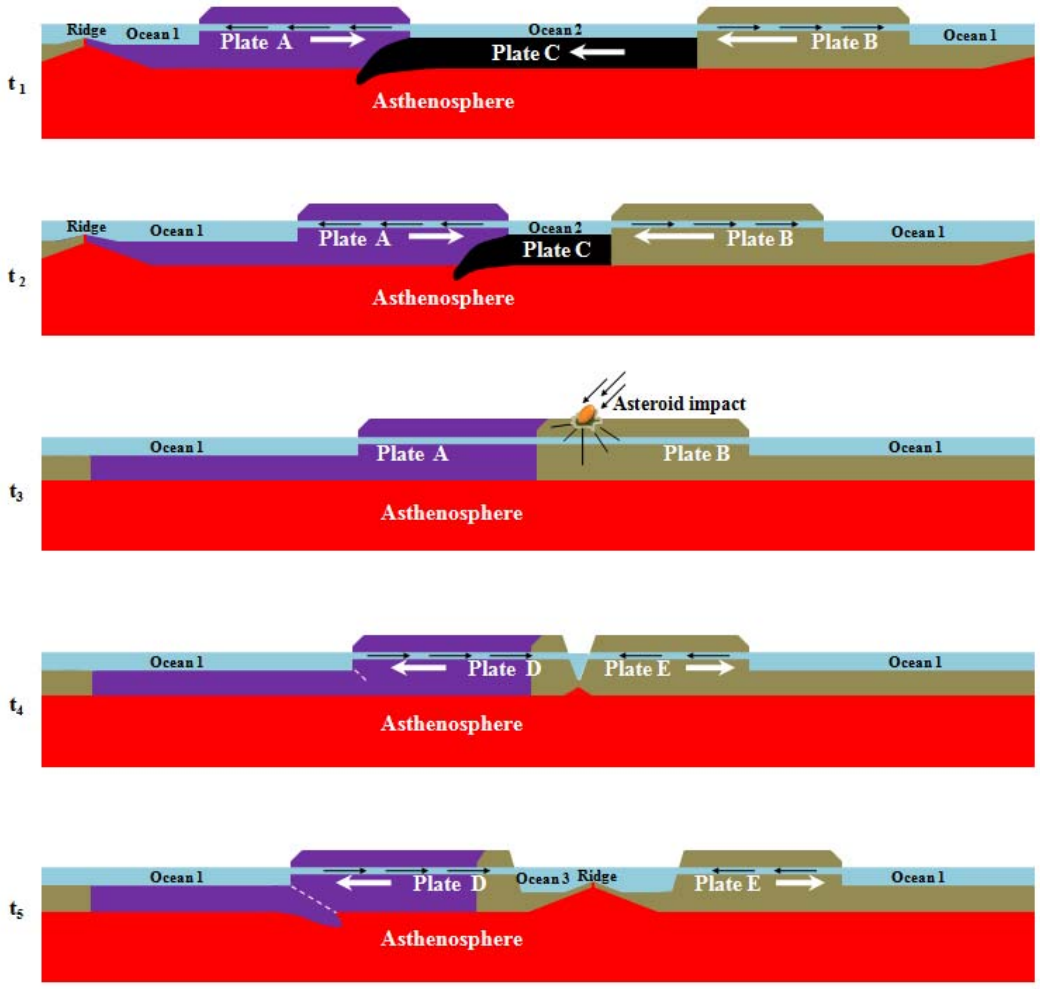

Figure 13. Modeling the dispersal and aggregation of plates. Back arrows in the passages denote water compensation from one ocean to another. Note that the ocean depth, plate size, and mantle are highly exaggerated.

Many people are extraordinarily perplexed as to why the Earth owns plate tectonics whereas the Venus does not. A lot of researches have shown that water provides the right conditions (maintaining a cool surface, for example) for plate tectonics, while the water's absence on Venus prohibits plate formation (Driscoll and Bercovici, 2013; Hilairet et al., 2007; Lenardic et al., 2008; Korenaga, 2007; Tozer, 1985; Lenardic and Kaula, 1994; Hirth and Kohlstedt, 1996; Landuyt and Bercovici, 2009). Our understanding of the kinematics and mechanics of ocean water provides additional solution to this issue: no water on Venus means no the contribution of ocean-generated force, and further no development of plate tectonics on the planet.

Acknowledgments

We express sincere thanks to Jinmin Chen for conducting the analysis of vector force and also to Bernhard Steinberger, Jeroen van Hunen, Maureen D. Long, and Thorsten Becker for their helpful comments on this research. The author declares that there is no conflict of interest. No funding is provided for this research.

Data Availability Statement

The movement data of 121 sample locations are from GSRM v.2.1 (Kreemer et al., 2014) and are available through UNAVCO (https://www.unavco.org/software/geodetic-utilities/plate-motion-calculator/plate-motion-calculator.html). The latitude and longitude of the controlling sites on the four continental plates in Figure 4 are made through ETOPO1 Global Relief Model (Amante and Eakins, 2009), and the ocean depths were artificially resolved through Bathymetric Data Viewer of NOAA (https://ngdc.noaa.gov/mgg/global/global.html). The tide data in Figure 11 are from GLOSS database (e.g., the Global Sea Level Observing System) (Caldwell et al. 2015).

References

Alvarez, L. W., Alvarez, W., Asaro, F., and Michel, H. V. (1980). Extraterrestrial cause for the Cretaceous-Tertiary extinction. *Science*, 208,1095-1108.

Amante, C., and Eakins, B. W. (2009). ETOPO1 1 Arc-Minute Global Relief Model: Procedures, Data Sources and Analysis. NOAA Technical Memorandum NESDIS NGDC-24. National Geophysical Data Center, NOAA. doi:10.7289/V5C8276M.

Alisic, L., Gurnis, M., Stadler, G., Burstedde, C., and Ghattas, O. (2012). Multi-scale dynamics and rheology of mantle flow with plates. *J. Geophys. Res*., 117, B10402, doi:10.1029/2012JB009234.

Becker, T. W., Faccenna, C. (2011). Mantle conveyor beneath the Tethyan collisional belt: Earth Planet. *Sci. Lett*., 310, 453-461.

Becker, T. W., and O'Connell, R. J. (2001). Predicting plate velocities with mantle circulation models. *Geochem. Geophys. Geosyst.*, 2, 2001GC000171.

Becker, T. W. (2017). Superweak asthenosphere in light of upper mantle seismic anisotropy. *Geochem. Geophys. Geosyst*., 18, doi:10.1002/ 2017GC006886.

Bercovici, D., Tackeley, P. J., and Ricard, Y. (2015). The generation of plate tectonics from mantle dynamics: Reference Module in Earth Systems and Environmental Science. *Treatise on Geophysics (Second Edition)*, 7, 271-318.

Berner. R. (2004). The Phanerozoic Carbon Cycle, Oxford University Press.

Bird, P., Liu, Z., Rucker, W. K. (2008). Stresses that drive the plates from below: definitions, computational path, model optimization, and error analysis. *J. Geophys. Res*., 113, B11406.

Bokelmann, G. H. R. (2002). Which forces drive North America? *Geology*, 30, 1027-1030.

Bott, M. H. P. (1993). Modeling the Plate-Driving Mechanism. *Journal of the Geological Society*, 150, 941-951.

Bott, M. H. P., Kusznir, N. J. (1984). The origin of tectonic stress in the lithosphere. *Tectonophysics*, 105, 1-13.

Brandmayr, E., Marson, I., Romanelli, F., & Panza, G. F. (2011). Lithosphere density model in Italy: no hint for slab pull. *Terra Nova*, 23, 292-299.

Cande, S. C., LaBrecque, J. L., Larson, R. L., Pitman, W. C., III, Golovchenko, X., and Haxby,W. F. (1989). Magnetic lineations of the world's ocean basins, Tulsa, Oklahoma. American Association of Petroleum Geologists.

Cande, S. C., Kent, D. V. (1992). A new geomagnetic polarity time scale for the Late Cretaceous and Cenozoic. *J. Geophys. Res*., 97(10), 13917-13951.

Caldwell, P. C., Merrfield, M. A., Thompson, P. R. (2015). Sea level measured by tide gauges from global oceans - the Joint Archive for Sea Level holdings (NCEI Accession 0019568), Version 5.5, NOAA National Centers for Environmental Information, Dataset, doi:10.7289/V5V40S7W.

Chapple, W. M., and Tullis, T. E. (1977). Evaluation of the forces that drive the plates. *J. Geophys. Res*., 82, 1969-1984.

Cloetingh, S., and Wortel, R. (1986). Stress in the Indo-Australian plate. *Tectonophysics*, 132, 49-67.

Coltice, N., Gerault, M., and Ulvrova, M. (2017). A mantle convection perspective on global tectonics. *Earth-Science Reviews*, 165, 120-150.

Condie, K. C. (2001). Mantle plumes and their record in Earth history. Cambridge University Press, Cambridge.

Conrad, C. P., Hager, B. H. (1999). The effects of plate bending and fault strength at subduction zones on plate dynamics. *J. Geophys. Res*., 104, 17551-17571.

Conrad, C. P., Lithgow-Bertelloni, C. (2002). How Mantle Slabs Drive Plate Tectonics. *Science*, 298 (5591), 207-09.

Conrad, C. P., & Lithgow-Bertelloni, C. (2003). How mantle slabs drive plate tectonics. *Science*, 298, 207-209.

Cruciani, C., Carminati, E., & Doglioni, C. (2005). Slab dip vs. lithosphere age: no direct function. *Earth and Planetary Science Letters*, 238, 298-310.

Dart, T. L., Zoback, M. L. (1987). *US Open File Rep*., 43, 87-283.

Doglioni, C., Ismail-Zadeh, A., Panza, G., Riguzzi, F. (2011). Lithosphere-asthenosphere viscosity contrast and decoupling. *Physics of the Earth and Planetary Interiors*, 189, 1-8.

Doglioni, C., and Panza, G. (2015). Polarized Plate Tectonics. *Advances in Geophysics*, 56,1-167.

Driscoll, P. and Bercovic, D. (2013). Divergent evolution of Earth and Venus: Influence of degassing, tectonics, and magnetic fields. *Icarus*, 226, 1447-1464.

Egbert, G. D., Ray, R. D. (2000). Significant dissipation of tidal energy in the deep ocean inferred from satellite altimeter data. *Nature*, 405, 775-778.

El Gabry, M. N., Panza, G. F., Badawy, A. A., & Korrat, I. M. (2013). Imaging a relic of complex tectonics: the lithosphere-asthenosphere structure in the Eastern Mediterranean. *Terra Nova*, 25(2), 102-109.

Faccincani, L., Faccini, B., Casetta, F., Mazzucchelli, M., Nestola, F., Coltorti, M. (2021), EoS of mantle minerals coupled with composition and thermal state of the lithosphere: Inferring the density structure of peridotitic systems. *Lithos*, 404-405, 106483.

Fleitout, L., Froidevaux, C. (1983). Tectonic stresses in the lithosphere. *Tectonics*, 2(3), 315-324.

Forsyth, D. & Uyeda, S. (1975). On the relative importance of the driving forces of plate motion. *Geophys. J. Int*., 43, 163-200.

Freed, A., Hashima, A., Becker,T. W., Okaya, D. A., Sato, H., and Hatanaka, Y. (2017). Resolving depth-dependent subduction zone viscosity and afterslip from postseismic displacements following the 2011 Tohoku-oki, Japan earthquake. *Earth Planet. Sci. Lett.*, 459, 279-290.

Frepoli, A., Selvaggi, G., Chiarabba, C., & Amato, A. (1996). State of stress in the Southern Tyrrhenian subduction zone from fault-plane solutions. *Geophysical Journal International*,125, 879-891.

Ghosh, A., Becker, T. W., Humphreys, E. D. (2013). Dynamics of the North American continent. *Geophys. J. Int*., 194, 651-669.

Ghosh, A., and Holt, W. E. (2012). Plate motions and stresses from global dynamic models. *Science*, 335, 839-843.

Gölke, M., and Coblentz, D. (1996). Origins of the European regional stress field. *Tectonophysics*, 266, 11-24.

Gripp, A. E., & Gordon, R. G. (2002). Young tracks of hotspots and current plate velocities. *Geophysical Journal International*, 150, 321-361.

Grünthal, G., and Stromeyer, D. (1992). The recent crustal stress field in central Europe: Trajectories and finite element modeling. *J. Geophys. Res*., 97(B8), 11, 805-11,820.

Gutenberg, B. (1956). The energy of Earthquakes. *Quart. J. Geol. Soc. London*, 112, 1-14.

Hager, B. H., and Richards, M. A. (1989). Long-wavelength variations in Earth's geoid: Physical models and dynamical implications. *Philosophical Transactions of the Royal Society of London, Series A*, 328, 309-327.

Hales, A. (1936). Convection currents in the Earth. *Monthly Notice of the Royal Astronomical Society, Geophysical Supplement*, 3, 372-379.

Hames, W. E., Renne, P. R., Ruppel, C. (2000). New evidence for geologically instantaneous emplacement of earliest Jurassic Central Atlantic magmatic province basalts on the North American margin. *Geology*, 28,859-862.

Hawley, W. B., Allen, R., and Richards, M. A. (2016). Tomography reveals buoyant asthenosphere accumulating beneath the Juan de Fuca plate. *Science*, 353, 1406-1408.

Heidbach, O., Rajabi, M., Cui , X. F., Fuchs, K., Müller, B., Reinecker, J., Reiter, K.,Tingay., M., Wenzel, F., Xie, F. R., Ziegler, M. O., Zoback, M., Zoback, M. (2018). The World Stress Map database release 2016: Crustal stress pattern across scales. *Tectonophysics*, 744, 484-498.

Heidbach, O., Reinecker, J., Tingay, M., Müller, B., Sperner, B., Fuchs, K., Wenzel, F. (2007). Plate boundary forces are not enough: Second- and third-order stress patterns highlighted in the World Stress Map database. *Tectonics*, 26, http://doi.org/10.1029/2007TC002133 (PDF).

Heidbach, O., Tingay, M., Barth, A., Reinecker, J., Kurfeß, D., Müller, B. (2010). Global crustal stress pattern based on the World Stress Map database release 2008. *Tectonophys*, 482, 3-15.

Heidbach, O., Rajabi, M., Reiter, K., Ziegler, M. (2016). World Stress Map 2016. GFZ Data Services, http://doi.org/10.5880/WSM.2016.002.

Hess, H. H. (1962). History Of Ocean Basins, in Engel, A. E. J., James, H. L., & Leonard, B. F., eds. Petrologic Studies: A volume in honor of A. F. Buddington. Boulder, CO, *Geological Society of America*, 599-620.

Hibsch, C., Jarrige, J-J., Cushing, E. M., Mercier, J. (1995). Paleostress analysis, a contribution to the understanding of basin tectonics and geodynamic evolution: example of the permian-cenozoic tectonics of Great Britain and geodynamic implications in Western Europe. Tectonophysics, 252, 103-136.

Hilairet, N., Reynard, B., Wang, Y., Daniel, I., Merkel, S., Nishiyama, N., and Petitgirard, S. (2007). High-Pressure Creep of Serpentine, Interseismic Deformation, and Initiation of Subduction. Science, 318(5858), 1910-1913.

Hirth, G. and Kohlstedt, D. (1996). Water in the oceanic upper mantle: Implications for rheology, melt extraction and the evolution of the lithosphere. *Earth and Planetary Science Letters*, 144, 93-108.

Holmes, A. (1931). Radioactivity and Earth Movements. *Nature*, 128, 496-496.

Holtzman, B. (2016). Questions on the existence, persistence, and mechanical effects of a very small melt fraction in the asthenosphere. *Geochem. Geophys. Geosyst*., 17, 470-484, doi:10.1102/2015GC006102.

Hu, Y., Bürgmann, R., Banerjee, P., Feng, L. J., Hill, E. M., Ito, T., Tabei, T., Wang, K. L. (2016). Asthenosphere rheology inferred from observations of the 2012 Indian Ocean earthquake. *Nature*, 538(7625), 368-372.

Isacks, B., & Molnar, P. (1971). Distribution of stresses in the descending lithosphere from a global survey of focal-mechanism solutions of mantle earthquakes. *Reviews of Geophysics*, 9, 103-174.

James, T. S., Gowan, E. J., Wada, L., and Wang, K. L. (2009). Viscosity of the asthenosphere from glacial isostatic adjustment and subduction dynamics at the northern Cascadia subduction zone, British Columbia, Canada. *Journal of Geophysical Research: Solid Earth*, 114(B4), CiteID B04405.

Jordan, T. H. (1974). Some comments on tidal drag as a mechanism for driving plate motions. *J. Geophys. Res*., 79, 2141-2142.

Kaufmann, G., and Lambeck, K. (2000). Mantle dynamics, postglacial rebound and the radial viscosity profile. *Physics of the Earth and Planetary Interiors*, 121, 301-324.

Kawakatsu, H., Kumar, P., Takei,Y., Shinohara, M., Kanazawa, T., Araki, E., and Suyehiro, K. (2009). Seismic evidence for sharp lithosphere asthenosphere boundaries of oceanic plates. *Science*, 324, 499-502.

Kido, M., Yuen, D. A., Cadek, O., and Nakakuki, T. (1998). Mantle viscosity derived by genetic algorithm using oceanic geoid and seismic tomography for whole mantle versus blocked-flow situations. *Physics of the Earth and Planetary Interiors*, 107, 307-326.

King, S. D. (1995). The viscosity structure of the mantle, In Reviews of Geophysics (Supplement) U.S. *Quadrennial Report to the IUGG* 1991-1994, 11-17.

Korenaga, J. (2007). Thermal cracking and the deep hydration of oceanic lithosphere: A key to the generation of plate tectonics?. *J. Geophys. Res*., 112(B5), DOI: 10.1029/2006JB004502.

Korenaga, J., Karato, S.-I. (2008). A new analysis of experimental data on olivine rheology. *J. Geophys. Res*., 113, B02403.

Kreemer, C., Blewitt, G., and Klein, E.C. (2014). A geodetic plate motion and Global Strain Rate Model. *Geochemistry, Geophysics, Geosystems*, 15, 3849-3889.

Kreemer, C., Holt, W. E., & Haines, A. J. (2002). The global moment rate distribution within plate boundary zones. *American Geophysical Union Geodynamics Series*, 30, 173-189.

Kusznir, N. J., & Bott, M. H. P. (1977). Stress concentration in the upper lithosphere caused by underlying viscoelastic creep. *Tectonophysics*, 43, 247-256.

Landuyt, W. and Bercovici, D. (2009). Variations in planetary convection via the effect of climate on damage. *Earth and Planetary Science Letter*, 277, 29-37.

Lenardic, A., Jellinek, M., and Moresi, L-N. (2008). A climate change induced transition in the tectonic style of a terrestrial planet. *Earth and Planetary Science Letters*, 271, 34-42.

Lenardic, A. and Kaula, W. (1994). Self-lubricated mantle convection: Two-dimensional models. *Geophysical Research Letters*, 21, 1707-1710.

Lithgow-Bertelloni, C., Richards, M. A. (1995). Cenozoic plate driving forces. *Geophys. Res. Lett*., 22, 1317-1320.

Lithgow-Bertelloni, C. (2014). Driving Forces: Slab Pull, Ridge Push. Encyclopedia of Marine Geosciences.

Ma, Z. J., Li, C. D., Gao, X. L. (1996). General characteristics of global tectonics in the Mesozoic and Cenozoic (in Chinese). *Geological Science and Technology Information*, 15(4), 21-25.

Marzoli, A., Renne, P. R., Piccirillo, E. M., Ernesto, M., Bellieni, G., de Min, A. (1999). Extensive 200-million-year-old continental flood basalts of the Central Atlantic magmatic province. *Science*, 284(5414),616-618.

McKenzie, D. P. (1968). The Influence of the Boundary Conditions and Rotation on Convection in the Earth's Mantle. *The Geophysical Journal*, 15, 457-500.

McKenzie, D. P. (1969). Speculations on the Consequences and Causes of Plate Motions. *The Geophysical Journal*, 18, 1-32.

Mei, S., Bai, W., Hiraga, T., and Kohlstedt, D. L. (2002). Influence of melt on the creep behavior of olivine basalt aggregates under hydrous conditions. *Earth and Planetary Science Letters*, 201, 491-507.

Middleton, G. V., Wilcock, P. R. (1996). Mechanics in the Earth and Environmental Sciences, Cambridge University Press, Australia , 496.

Miller, G. R. (1996). The flux of tidal energy out of the deep oceans. *J. Geophys. Res*., 71, 2485-2489.

Mitrovica, J. X. (1996). Haskell (1935) revisited. *J. Geophys. Res*., 101, 555-569.

Mojzsis, S. J., Harrison, T. M., and Pidgeon, R. T. (2001). Oxygen-isotope evidence from ancient zircons fro liquid water at the Earth's surface 4,300 Myr ago. *Nature*, 409(6817):178-181.

Morgan, W. J. (1972). Deep mantle convection plumes and plate motions. *Bull. A. Pet. Geol*., 56, 203-213.

Müller, B., Zoback, M. L., Fuchs, K., Mastin, L., Gregersen, S., Pavoni, N., Stephansson, O., Ljunggren, C. (1992). Regional patterns of tectonic stress in Europe. *J. Geophys. Res.*, 97(B8), 11,783-11,803.

Munk, W. (1968). Once again-tidal friction. *Quarterly Journal of the Royal Astronomical Society*, 9, 352-375.

Naif, S., Key, K., Constable, S., and Evans, R. L. (2013). Melt-rich channel observed at the lithosphere-asthenosphere boundary. *Nature*, 495, 356-359.

Naliboff, J. B., Lithgow-Bertelloni, C., Ruff, L. J., de Koker, N. (2012). The effects of lithospheric thickness and density structure on Earth's stress field. *Geophysical Journal International*, 188, 1-17.

Oxburgh, E. and Turcotte, D. (1978). Mechanisms of continental drift. *Reports on Progress in Physics*, 41, 1249-1312.

Panza, G. F., Peccerillo, A., Aoudia, A., & Farina, B. (2007). Geophysical and petrological modeling of the structure and composition of the crust and upper mantle in complex geodynamic settings: the Tyrrhenian Sea and surroundings. *Earth-Science Reviews*, 80, 1-46.

Parsons, B., Richter, F. M. (1980). A relation between the driving force and geoid anomaly associated with mid-ocean ridges. *Earth and Planetary Science letters*, 51, 445-450.

Perkeris, C. (1935). Thermal convection in the interior of the Earth. *Monthly Notices of the Royal Astronomical Society, Geophysical Supplement*, 3, 343-367.

Pollitz, F. F., Bürgmann, R., & Romanowicz, B. (1998). Viscosity of oceanic asthenosphere inferred from remote triggering of earthquakes. *Science*, 280, 1245-1249.

Prinn, R. G., Fegley, B. (1987). Bolide impacts, acid rain, and biospheric traumas at the Cretaceous-Tertiary boundary. *Earth and Planetary Science Letters*, 83,1-15.

Raymond, C. A., Stock, J, M., Cande, S. C. (2000). Fast Paleogene motion of the Pacific hotspots from revised global plate circuitcon straints. *Geophysical Monography*, 121, 359-375.

Rampino, M. R., Stothers, R. B. (1984). Geological rhythm and cometary impacts. Sciences, 226(4681),1427-1431.

Reynard, B., Hilairet, N., Wang, Y., Daniel, I., Merkel, S., Petitgirard, S., Nishiyama, N. (2007). High-pressure creep of serpentine, interseismic deformation, and initiation of subduction. *Science*, 318(5858), 1910-1913.

Ricard, Y., Fleitout, L., Froidevaux. C. (1984). Geoid heights and lithospheric stresses for a dynamic earth. *Ann. Geophys*, 2, 267- 286.

Richardson, R. M. (1992). Ridge Forces, Absolute Plate Motions, and the Intraplate Stress Field. *J. Geophys. Res*., 97, 11739-11748.

Richardson, R. M., and Cox, B. L. (1984). Evolution of oceanic lithosphere: A driving force study of the Nazca Plate. *Journal of Geophysical Research: Solid Earth*, 89 (B12), 10043-10052.

Richardson, R. M., and Reding, L. (1991). North American plate dynamics. *J. Geophys. Res*., 96, 12201-12223.

Richardson, R. M., Solomon, S. C., and Sleep, N. H. (1979). Tectonic stress in the plates. *Rev. Geophys*., 17, 981-1019.

Riguzzi, F., Panza, G., Varga, P., Doglioni, C. (2012). Can Earth's rotation and tidal despinning drive plate tectonics?. *Tectonophysics*, 484, 60-73.

Rochester, M. G. (1973). The Earth's rotation. *EOS, T rans. Am. geophys. Un.*, 54, 769-780.

Runcorn, S. (1962a). Towards a theory of continental drift. *Nature*, 193, 311-314.

Runcorn, S. (1962b). Convection currents in the Earth's mantle. *Nature*, 195, 1248-1249.

Russo, R. M., & Silver, P. G. (1994). Trench-parallel flow beneath the Nazca plate from seismic anisotropy. *Science*, 263, 1105-1111.

Scoppola, B., Boccaletti, D., Bevis, M., Carminati, E., Doglioni, C. (2006). The westward drift of the lithosphere: A rotational drag?. *GSA Bulletin*, 118, 199-209.

Slomon, S. C., Sleep, N. H., and Richardson, R. M. (1975). On the forces driving plate tectonics: Inferences from absolute plate velocities and intraplate stress. *Geophys. J. R. Astron. Soc*., 42, 769-801.

Spence, W. (1987). Slab pull and the seismotectonics of subducting lithosphere. *Reviews of Geophysics*, 25 (1), 55-69.

Sperner, B., Müller, B., Heidbach, O., Delvaux, D., Reinecker, J., Fuchs, K. (2003). Tectonic stress in the Earth's crust: advances in the World Stress Map project, in New insights in structural interpretation and modelling, edited by D. A. Nieuwland, Special Publication 212, 101-116, Geol. Soc. Spec. Pub., London.

Stadler, G., Gurnis, M., Burstedde, C., Wilcox, L. C., Alisic, L., Ghattas, O. (2010). The dynamics of plate tectonics and mantle flow: from local to global scales. *Science*, 329, 1033-1038.

Stefanick, M., and Jurdy, D. M. (1992). Stress observations and driving force models for the South American plate. *J. Geophys. Res*., 97, 11905-11913.

Stern, T. A., Henrys, S. A., Okaya, D., Louie, J. N., Savage, M. K., Lamb, S., Sato, H., Sutherland, R., and Iwasak, T. (2015). A seismic reflection image for the base of a tectonic plate. *Nature*, 518, 85-88.

Steinberger, B., Schmeling, H., Marquart, G. (2001). Large-scale lithospheric stress field and topography induced by global mantle circulation. *Earth Planet. Sci. Lett*., 186, 75-91, doi:10.1016/S0012-821X(01)00229-1

Steinberger, B. (2016). Topography caused by mantle density variations: observation-based estimates and models derived from tomography and lithosphere thickness. *Geophys. J. Int*., 205, 604-621.

Squyres, S. W., Grotzinger, J. P., Arvidson, R. E., Bell III, J. F., Calvin, W., Christensen, P. R., Clark, B. C., Crisp, J. A., Farrand, W. H., Herkenhoff, K. E., Hohnson, J. R., Klingelhöfer, J., Knoll, A. H., Mclennan, S. M., Mcsween JR, H. Y., Morris, R. V., Rice JR, J. W., Rieder, R., and Soderblom, L. A. (2004). In situ evidence for an ancient aqueous environment at Meridiani Planum, Mars. *Science*, 306(5702), 1709-1714.

Tanimoto, T., Lay, T. (2000). Mantle dynamics and seismic tomography. *Proceedings of the National Academy of Sciences*, 97 (23), 12409-12410.

Tozer, D. (1985). Heat transfer and planetary evolution. *Geophysical Surveys*, 7, 213-246.

Turcotte, D. L., and Oxburgh, E. (1972). Mantle convection and the new global tectonics. *Annual Review of Fluid Mechanics*, 4, 33-66.

Turcotte, D. L., & Schubert, G. (2002). Geodynamics. Cambridge University Press, Cambridge.

Turcotte, D. L., Schubert, G. (2014). Geodynamics (Third Edition), Cambridge University Press, Cambridge.

Tutu, A. O., Steinberger, B., Sobolev, S. V., Rogozhina, I., Popov, A. A. (2018). Effect of upper mantle heterogeneities on lithospheric stress field and dynamic topography. *Solid Earth*, 9, 649-668, doi:10.5194/se-9-649-2018

Ulmer, P., & Trommsdorff, V. (1995). Serpentine stability to mantle depths and subduction related magmatism. *Science*, 268, 858-861.

Valley, J. W., Peck, W. H., King, E. M., and Wilde, S. A. (2002). A cool early earth. *Geology*, 30(4): 351-354.

Vigny, C., Ricard, Y., Froidevaux, C. (1991). The Driving Mechanism of Plate Tectonics. *Tectonophysics*, 187, 345-360.

Vine, F. J., & Matthews, D. H. (1963). Magnetic Anomalies Over Oceanic Ridges. *Nature*, 199, 947-949.

Walker, J., Hays, J., and Kasting, J. (1981). A negative feedback mechanism for the long-term stabilization of Earth's surface temperature. *J. Geophys. Res*., 86: 9776-9782.

Wan, T. F. (1993). Tectonic stress field and its application to the intraplate in Eastern China (in Chinese). Beijing, Geological Publishing Company, 1-103.

Wan, T. F. (2018). On the dynamic mechanics of global lithosphere plate tectonics (In Chinese). *Earth Science Frontiers*, 25, DOI:10.13745/j.esf.sf.2018.1.1.

Wegener, A. (1915). The Origin of Continents and Oceans, New York, NY, Courier Dover Publications.

Wegener, A. (1924). The origin of continents and oceans (Entstehung der Kontinente und Ozeane), Methuen & Co.

White, R., McKenzie, D. (1989). Magmatism at rift zones: The generation of volcanic continental margins and flood basalts. *J. Geophys. Res*., 94, 7685-7729.

Wilson, J. T. (1963). A possible origin of the Hawaiian Island. *Canada Journal of Physics*, 41, 863-868.

Wortel, R., and Cloetingh, S. (1981). On the origin of the Cocos-Nazca spreading center. *Geology*, 9, 425-430.

Zhong, S. (2001). Role of ocean-continent contrast and continental keels on plate motion, net rotation of lithosphere, and the geoid. *J. Geophys. Res*., 106, 703-712.

Zoback, M. L., and Burke, K. (1993). Lithospheric stress patterns: A global view. Eos Trans. AGU, 74, 609-618.

Zoback, M. L., Zoback, M. D., Adams, J., Assumpção, M., Bell, S., Bergman, E. A., Blümling, P., Brereton, N. R., Denham, D., Ding, J., Fuchs, K., Gay, N., Gregersen, S., Gupta, H. K., Gvishiani, A., Jacob, K., Klein, R., Knoll, P., Magee, M., Mercier, J. L., Müller, B. C., Paquin, C., Rajendran, K., Stephansson, O., Suarez, G., Suter, M., Duias, A., Xu, Z. H., Zhi, Z. M. (1989). Global patterns of tectonic stress. *Nature*, 341, 91-298.

Zoback, M. L., Magee, M. (1991). Stress magnitudes in the crust: constraints from stress orientation and relative magnitude data. *Philosophical Transactions of the Royal Society, London*, A337(1645), 181-194.

Zoback, M. L. (1992). First- and Second-Order Patterns of Stress in the Lithosphere: The World Stress Map Project. *J. Geophys. Res*., 97(B8), 11703-11728.

Zoback, M. D., and Zoback, M. L. (1991). Tectonic stress field of North America and relative plate motions, In Neotectonics of North America, Decade Map vol. I, edited by D. B. Slemmons et al., 339-366, Geol. Soc. of Am., Boulder, Colo.